NUMERICAL INVESTIGATION ON SHEAR BEHAVIOUR OF OLD-TO-NEW CONCRETE INTERFACE WITH RECTRANGULAR ROUGHNESS TOOTH

TEY YEE CHEAN

UNIVERSITI TUNKU ABDUL RAHMAN

NUMERICAL INVESTIGATION ON SHEAR BEHAVIOUR OF OLD-TO-NEW CONCRETE INTERFACE WITH RECTANGULAR ROUGHNESS TOOTH

TEY YEE CHEAN

A project report submitted in partial fulfilment of the requirements for the award of Bachelor of Civil Engineering with Honours

Lee Kong Chian Faculty of Engineering and Science
Universiti Tunku Abdul Rahman

May 2024

DECLARATION

I hereby declare that this project report is based on my original work except for citations and quotations which have been duly acknowledged. I also declare that it has not been previously and concurrently submitted for any other degree or award at UTAR or other institutions.

Signature : 

Name : Tey Yee Chean

ID No. : 1901950

Date : 16/5/2024

APPROVAL FOR SUBMISSION

I certify that this project report entitled **"NUMERICAL INVESTIGATION ON SHEAR BEHAVIOUR OF OLD-TO-NEW CONCRETE INTERFACE WITH RECTANGULAR ROUGHNESS TOOTH"** was prepared by **TEY YEE CHEAN** has met the required standard for submission in partial fulfilment of the requirements for the award of Bachelor of Civil Engineering with Honours at Universiti Tunku Abdul Rahman.

Approved by,

Signature	:	
Supervisor	:	Dr. Woon Kai Siong
Date	:	16/5/2024

ACKNOWLEDGEMENTS

I extend my gratitude to all those who contributed to the successful completion of this project. A special acknowledgement is due to my research supervisor, Dr. Woon Kai Siong, for his uncompromising support, invaluable advice, and guidance throughout the research process. His expertise, patience, and encouragement played a pivotal role in shaping the outcome of this study.

I am also appreciative of the persistent love and support from my parents, whose encouragement served as a driving force and kept me motivated to strive through the challenges encountered during this project.

Lastly, I would like to express my thanks to my friends for their continuous support, encouragement, and understanding during difficult times. Their words of positivity and motivation were a source of strength that kept me going.

ABSTRACT

The interface between old and new concrete in structural extension and repair is crucial for maintaining structural integrity and load-bearing capacity. Previous studies have focused on the impact of surface roughness texture on the behaviour of the concrete-to-concrete interface, but there is limited research on the effect of manipulating the roughness tooth parameter on the shear behaviour. To address this research gap, this study conducts a numerical investigation to examine the effectiveness of rectangular roughness tooth on the shear behaviour of the old-to-new concrete interface. This study used a double shear test setup and the finite element method to conduct a parametric study, exploring the relationship between tooth thickness and shear capacity, as well as the effect of confining pressure on the effectiveness of the rectangular tooth. The concrete interface parameter is calibrated using two reference specimens, followed by 18 test specimens with varying roughness tooth thickness (ranging from 30 mm to 70 mm) to conduct the parametric study. The findings indicate that increasing the tooth thickness positively impacts the ultimate shear capacity of the concrete interface. Specifically, there is a significant increase of 15.81% for the specimen batch without confining pressure and 14.87% for the specimen batch with confining pressure as tooth thickness increased from 30 mm to 70 mm. These results are supported by high coefficients of determination (R^2) of 0.9206 and 0.9976, respectively. Additionally, the presence of confining pressure leads to an average increase of 19% in shear capacity. Interestingly, the results demonstrate that the existence of confining pressure does not affect the degree of influence of tooth thickness on shear strength, as the increase in ultimate shear capacity in both batches is not significantly different. Hence, it underscores the importance of considering the tooth thickness, when designing the surface roughness texture of concrete in structural extension and repair projects to achieve optimal structural performance.

TABLE OF CONTENTS

LIST OF TABLES

LIST OF FIGURES

LIST OF SYMBOLS / ABBREVIATIONS

f'_c	concrete cylinder compressive strength, MPa
f_{b0}	initial equibiaxial compressive yield stress
f_{c0}	initial uniaxial compressive yield stress
f_{cm}	concrete compressive strength
f_{ctm}	concrete tensile strength
f_{cu}	concrete cube compressive strength, MPa
k_c	ratio of the second stress invariant on the tensile meridian to that on the compressive meridian
w	crack opening
A	interface area, mm^2
E_{cm}	elastic stiffness of concrete
G_F	fracture energy
K	stiffness coefficients
K_s	interface stiffness
P	shear load, N
S_{max}	interface shear strength at crack initiation
$\widetilde{\varepsilon_c^{in}}$	inelastic strains
δ_s^{init}	displacement at crack initiation
ε_{oc}^{el}	elastic strain
δ_c	damage initiation displacement
δ_m	total/plastic displacement
ε	flow potential eccentricity
ε_{c1}	plastic strain under compression
ε_{cr}	cracking strain
ε_{cu1}	ultimate strain under compression
μ	viscosity parameter
σ_c	uniaxial compressive stress
σ_{ct}	uniaxial tensile stress, MPa
σ_t	uniaxial compressive stress, MPa
τ	normalized shear stress, MPa

ψ	dilation angle in degrees
C3D8R	three-dimensional solid deformable parts and meshed with solid elements
CDP	concrete damage plasticity
FEA	finite element analysis
FEM	finite element method
LVDT	linear variable differential transducer
UHPC	ultra high-performance concrete

LIST OF APPENDICES

CHAPTER 1

INTRODUCTION

1.1 General Introduction

Concrete is a common material that has been used widely in the construction industry due to its toughness, durability, cost effectiveness and high strength properties. Basically, cement, water and aggregate are the most common components of concrete. Sometimes admixtures are added to the concrete to manipulate its properties to achieve a particular desired function. Recently, the engineers have prioritised the repair and strengthening of existing structures to further reduce construction costs and reuse the old structure without demolition. The idea of attaching the new concrete to the existing concrete structure has therefore become more important.

The bonding between the existing concrete surface and the new concrete surface is a significant concern, as the composite concrete structure may not have the durability of the one-time casting concrete. In addition, the internal force that should be considered most is the shear force that acts along the concrete and results in the crack or split at this interface. By accessing the behaviour of the concrete interface under the shear loading condition, it can help to deduce a proper manipulation of this concrete interface in order to reduce the impact of this interface on the overall strength of the entire concrete structure.

As noted by Furlong (n.d.), shear force is a force acting perpendicular to the longitudinal axis of structural members. For example, for a uniformly distributed load on a supported beam, the shear force will be greatest near the support. Figure 1.1 illustrates how a shear stress acts as an internal stress in response to the applied load and acts on a beam segment. Therefore, shear behaviour is the response of concrete to the shear stress, and it can be represented by various parameters such as ultimate shear capacity, failure locations and crack patterns.

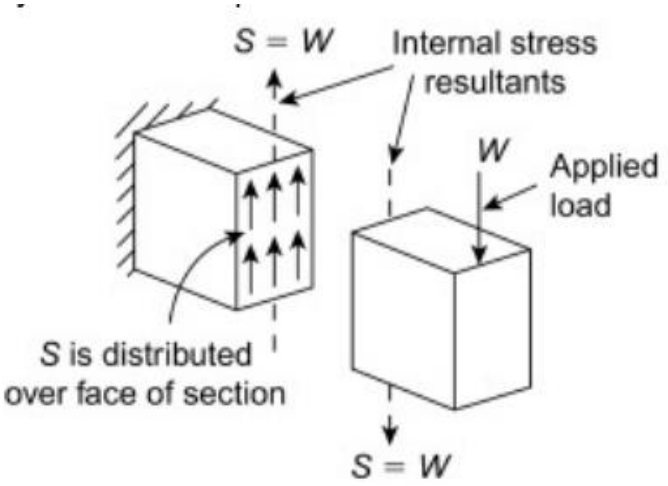

Figure 1.1: Shear Force Illustration Showcase (Parasher, 2022).

The concrete interface is considered to be the most vulnerable part of a composite concrete structure. According to Zhou, Micklebrough and Li (2005), the concrete interface will fail first before the individual concrete part starts to crack or crush under deflection, and it will have the significant impact on the overall structural performance. Especially under heavy loads, the overall performance of the concrete structure will be largely dependent on the interface. However, this weakness can be eliminated by increasing the effectiveness of the load transfer between the two connected concrete parts and by increasing their cohesiveness through the use of higher strength concrete, the addition of roughness tooth, the addition of adhesive agent in the interface or other appropriate means.

This paper presents an extension investigation done by Wu, Ayinde and Zhou (2023) which used the triangular roughness tooth. This study explored a different direction by manipulating the geometry of the roughness tooth to rectangular to investigate how well the load transfer in the interface compared to the triangular tooth. This study used a numerical approach to investigate the effect of a single rectangular tooth on the shear behaviour of a concrete interface. In this study, ABAQUS software was used to simulate the behaviour of the composite concrete under the designated condition.

1.2 Importance of the Study

Investigating the effect of shear stress on the concrete interface is important because the concrete interface is mainly affected by shear stress but not compression and it will affect the shear capacity of the whole structure. To abstract from a real-life example, the old-to-new concrete composition can be found in the construction industry where the concrete continues to be poured next to the half-cast concrete beam. This type of casting technique is quite common when casting for the massive concrete structure.

As stated by He et al. (2017), the texture of the interface is a highly relevant factor that affects the shear behaviour of the concrete-to-concrete bond. However, Wu, Ayinde, and Zhou (2023) only investigated how a single triangular roughness tooth can affect the shear behaviour of the concrete interface. Therefore, it is necessary to further investigate a different shape of roughness tooth to examine whether there is other shape is more feasible than the triangular roughness tooth.

Furthermore, this investigation provided an optimal parameter of the concrete interface with a rectangular roughness by studying the relationship between the tooth thickness and the shear capacity. Through analysing the response of the interface to the shear stress, the better tooth geometry between triangle and rectangle can be identified. Besides that, this numerical investigation allowed a quick and detailed exploration of design parameters before proceeding to a physical experiment.

In addition, the investigation of the shear force at the concrete interface by numerical analysis offered additional advantages over traditional experimental methods, such as cost effectiveness and no material consumption. By performing the simulations using software, the complex scenarios were analysed in less time and without the need for material consumption. Simulations can also be used to quickly evaluate different alternative scenarios. Numerical simulation can provide a rough estimate of the overall relationship between tooth thickness and interface shear capacity. The numerical results can also help to estimate the failure and shear capacity of the specimen in the physical experiment.

1.3 Problem Statement

Existing studies (Ayinde, Wu and Zhou, 2022; Ayinde et al., 2022; He et al., 2017; Wu, Ayinde and Zhou, 2023) had shown that a rougher interface can help to increase both the bond strength and the shear capacity of the interface. Other researchers (Ahmed and Aziz, 2019; Feng et al., 2021; Niwa et al., 2016; Yuan et al., 2021) also have carried out various analyses of the factors that can affect the strength of concrete interfaces, such as the use of ultra-high-performance concrete (UHPC), adhesive, fibre addition and reinforcement bars.

Wu, Ayinde and Zhou (2023) had focused their study on the triangular roughness tooth. The authors found that the angle and depth of the triangular tooth can influence the surface roughness at the tooth area and further increased the strength of the concrete interface compared to a flat surface. However, the study did not show the influence of the other geometry such as the rectangular tooth. The question should be whether the rectangular tooth would increase the roughness of the interface or act as a hinge support at the interface.

Although several efforts have been made to control the interface roughness geometry, it is extremely rare to find research that investigates how the geometric parameters of the roughness tooth have either an effective or ineffective influence on the shear behaviour of the concrete interface. In addition, the effect of different tooth shapes on shear behaviour has not yet been explored. As a result, it is a new research topic to investigate how a rectangular roughness tooth can either positively or negatively affect the shear capacity of the interface.

It is also important to consider the influence of confining pressure on the effectiveness of the roughness tooth. Wu, Ayinde and Zhou (2023) found that the specimens without confining pressure would have a much lower shear capacity than the specimens with confining pressure. Therefore, it is also important to investigate the shear behaviour of the concrete interface with a single rectangular roughness tooth in two different scenarios: with and without confining pressure. In order to save time and get a quick view of the specimen response before proceeding to physical laboratory testing, the Finite Element Method (FEM) was used. This method provides an alternative solution to investigate the shear behaviour of the concrete interface with a single rectangular roughness tooth without wasting material and saving time.

1.4 Aim and Objectives

The aim of this study is to conduct an investigation of the effectiveness of a single rectangular roughness tooth on the shear behaviour of the concrete interface. The objectives of the study are listed below:

(i) To develop the numerical model that accurately simulates the double shear test results.

(ii) To acquire the failure mode, crack patterns and normalised shear strength for each specimen.

(iii) To identify the relationship between the thickness of the rectangular roughness tooth and the shear behaviour of the old-to-new concrete interface, considering scenarios both with and without the application of confining pressure.

1.5 Scope and Limitation of the Study

The scope of this investigation is to investigate the effectiveness of a rectangular roughness tooth. The Finite Element Method (FEM) is used for this purpose, which involves the use of software to generate and simulate results. As part of the FEM, Finite Element Analysis (FEA) software was used to analyse the response and deformation of the concrete specimen. Specifically, ABAQUS software was used to simulate the double shear test to access the concrete interface. The limitations of this study are considered and stated below:

(i) The study only considers a single rectangular roughness tooth at the concrete interface.

(ii) The study only investigates the effect of the rectangular roughness tooth thickness and confining pressure on the shear behaviour of the interface.

(iii) The concrete strength is 28.0 MPa for old concrete parts and is 43.0 MPa for new concrete part.

(iv) The specimens do not have the presence of steel bars as reinforcement.

(v) The proposed confining pressure acting on specimen is 0 MPa and 1.0 MPa.

1.6 Contribution of the Study

By analysing the influence of the tooth thickness on the shear capacity, this study offers valuable insights that can have various societal benefits. Firstly, in terms of the construction industry, the outcomes of this study have the potential to enhance the efficiency of design and construction processes related to structural extensions and repairs involving concrete interfaces. Through an examination of geometric parameters such as tooth thickness, engineers can optimize their methods, resulting in more resilient and effective designs. Consequently, this optimisation can reduce the necessity for frequent maintenance and repairs, leading to long-term cost savings and promoting the sustainability of construction practices.

Moreover, this research demonstrates technological advancement by using the numerical simulation approach through the finite element method. By utilising computational tools, this study illustrates how numerical methods can reduce material wastage and cost expenditures in investigating the shear behaviour of concrete interfaces, as opposed to physical experiments, as long as the reliability of the numerical model is ensured.

1.7 Outline of the Report

Chapter 1 provides a general overview of concrete and the concept of shear force. In addition, this chapter also emphasises the importance of this research topic and highlights the problem statement which serves as the main direction for this research report. Moreover, this chapter outlines the objectives, scope, and limitations of this study.

Chapter 2 describes an extensive literature review that offers valuable insights into the research that had been done to investigate the concrete interface and provides recommendations for this study. Related papers were critically evaluated factors that impact the shear behaviour of concrete interfaces and the reliability of numerical modelling method.

Chapter 3 outlines an overview of the methodology used to perform the numerical investigation. This chapter also describes the specifications of the reference specimens and test specimens. The modelling process consideration and the detailed parameters to be input into ABAQUS software were described

in this chapter. This chapter also lists out the results that will be extracted from the finite element model after the numerical simulation.

Chapter 4 discusses the results obtained from the simulation carried out using the ABAQUS software. The normalised shear stress-slip curves, the maximum principal stress contour and the DAMAGET contour for all specimens were discussed in this chapter. The relationship between normalised shear capacity and tooth thickness was being analysed, plotted and discussed.

Chapter 5 summarises the outcomes discussed in Chapter 4. It also evaluates the aim and objectives achievements that determine the successful completion of the investigation. Furthermore, this chapter provides three recommendations for future research studies.

CHAPTER 2

LITERATURE REVIEW

2.1 Introduction

As noted by Zhou, Micklebrough and Li (2005), the overall performance and durability of composite concrete structure are highly dependent on the interfacial strength of the two different aged concrete parts, as the bond between the different aged concrete parts is much weaker compared to that of the one-time casting concrete. This weak bond of the interface will lead to problems such as cracking or slipping and will have a tragic effect on the structural integrity over time.

There are several factors that influence the shear, bond, and strength behaviour of the concrete interface. According to Xia et al. (2021), the addition of reinforcement or confining pressure can help to increase the ultimate shear capacity and interfacial cracking stress of the concrete interface. In addition, Feng et al. (2021) found that the bond strength between UHPC and normal concrete is strongly influenced by surface roughness, water/binder ratio and fibre type. Hence, this chapter presents a literature review on the factors that influence the shear behaviour of the concrete interface and the finite element method (FEM) used in previous studies (Wu, Ayinde and Zhou, 2023; Shamass, Zhou and Alfano, 2015; Ayinde et al., 2022) to investigate the shear behaviour of the concrete interface.

2.2 Factors Affecting the Interfacial Strength of Concrete

In recent years, the factors that can potentially affect the strength of the concrete interface have received considerable research attention. The influence of these factors on the strength of the concrete interface has been investigated under various conditions. Existing studies have investigated the effect of a single triangular roughness tooth (Wu, Ayinde and Zhou, 2023), a grooved surface (Wu, Ayinde and Zhou, 2022), the addition of fibres (Yuan et al., 2021) and the adhesives (Ahmed and Aziz, 2019). The different factors that have been manipulated have different effectiveness in increasing the interfacial strength of concrete structures.

2.2.1 Grooved Surface with Multiple Triangular Roughness Tooth

Wu, Ayinde and Zhou (2022) experimented with double-sided shear specimens to investigate the effect of a grooved surface on the shear behaviour of the concrete interface. The composite concrete specimen was cast in an old-new-old configuration and the test used in the experiment is double shear test. The manipulated parameter set in the research was the roughness tooth pattern and angle with constant roughness tooth depth.

According to the authors, the use of quantitative roughness brought a huge improvement in the interface cracking stress capacity and ultimate stress capacity. However, the authors also stated that increasing the number of roughness tooth did not help to increase the interface shear strength but had a negative effect on it. Referring to Figure 2.1, the experimental result with different grooved surface patterns was shown in this graph. The different interface types showed different curve slopes representing the different stiffness of the interface. All the specimens showed the elastic behaviour as the shear stress is directly proportional to the relative slip and fail directly without any residual resistance. Furthermore, the specimen with the best ultimate shear stress capacity is specimen DI_B. The surface pattern of this specimen is shown in Figure 2.2.

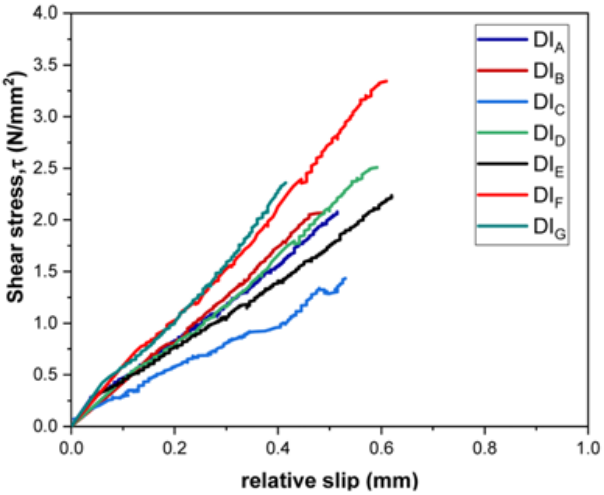

Figure 2.1: Shear Slip Curve of Different Grooved Surface Pattern Specimens (Wu, Ayinde and Zhou, 2022).

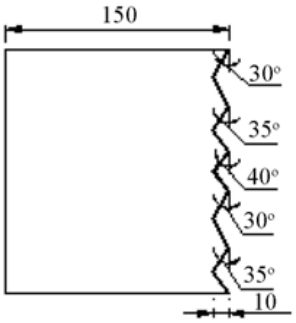

Figure 2.2: Specimen DC_B (Wu, Ayinde and Zhou, 2022).

Overall, the most significant finding of this study was that the different patterns of a grooved surface will have a different effect on the interface roughness. This is because the pattern of the grooved interface will affect the load transfer between two concrete parts. In a main idea, the more the grooved interface interferes, the more effective the load transfer capability and this capability can provide a higher ultimate shear capacity. In addition, the larger the tooth contact area at the interface, the more friction the interface will have. Thus, this relationship showed that a larger contact area can improve the shear strength of the interface.

2.2.2 Interfacial Roughness with Texture

He et al. (2017) had conducted research to study the relationship between the surface roughness parameter and the bonding of a old-to-new concrete. Some of the examples of roughness texture morphologies had been shown in Figure 2.3. The authors used these different types of roughness texture to find out the key aspect in the texture that can help improve the bond strength between two different aged concretes.

Figure 2.3: Pattern of Roughness Texture on Concrete Surface (He et al., 2017).

The result of the study indicated that there is a positive influence of the fractal dimension of concrete interfaces on mechanical properties. Specifically, an increase in the interfacial fractal dimension led to an increase in the mechanical strength of old-to-new concrete. This random roughness interface worked by the same mechanism as a grooved surface, increasing the contact area to increase the friction of the interface, resulting in higher shear strength.

In conclusion, this study of the influence of a coarser interface on concrete bonding has shown that interface roughness can help to increase the interfacial strength. However, a more detailed study of the bonding behaviour of the interface with consideration of the roughness tooth is required.

2.2.3 Fibre Addition

Yuan et al. (2021) conducted research to investigate the effects of several factors on the bonding behaviour between new and old concrete, including fibre addition, new concrete strength grade, interface angle and type of surface treatment. Figure 2.4 shows the illustration of I-shaped specimen to be used for the axial tensile test to investigate efficiency by manipulating several aspects at the interface.

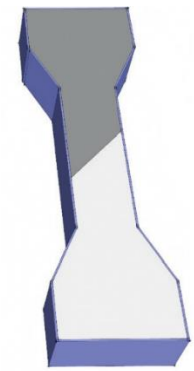

Figure 2.4: Axial Tensile Test Specimen (Yuan et al., 2021).

The study found that the use of steel and polypropylene fibres can significantly improve the axial tensile bond behaviour of the concrete interface. The maximum bond strength was obtained when the specimen contained 0.25% by volume of steel fibres. Yuan et al. (2021) claimed that adding fibres only to the interface region of the old concrete is a better method to improve the bond strength at the concrete interface.

Overall, this study has demonstrated the effect of fibre addition on the bonding behaviour of the interface between fresh and aged concrete under tensile conditions. However, there is still room for further research into the combination of roughness tooth at the concrete interface and fibre reinforcement. Additionally, the shear behaviour is also an important behaviour that should be investigated. Such a study will provide a better understanding of the compatibility, mechanisms of reaction of concrete under different conditions such as tension, compression or bending.

2.2.4 Key-Joints

Zhou, Micklebrough and Li (2005) investigated the shear behaviour, shear capacity and shear transfer mechanism of key joints. Four different types of joints were considered in the study: single key joints and triple key joints, which were further subdivided into dry joints and epoxy joints.

This study found that the shear strength of the keyed joint is not positively influenced by the number of keys in a dry joint, but rather negatively influenced by it. Due to fitting imperfections in multi-keyed joints, the shear transmission is not in good condition. As a result, the shear capacity of triple-keyed dry joints is lower than that of single-keyed dry joints.

Moreover, Ahmed and Aziz (2019) also conducted a related study in recent years, focusing on the behaviour and feasibility of multi-key joints under shear force. The authors examined the cracking and failure behaviour of the joints and reported the results of experimental tests on different types of joints, including the consideration of dry and epoxy joints.

The authors also looked at how various elements, such as the number of shear keys and the presence of flange keys, affect the shear capacity and load transfer performance of the joints. The findings are also consistent with those of Zhou, Micklebrough and Li (2005) that there was no significant increase in the elasticity of dry joints when the number of keys was increased. However, the inclusion of shear keys in a flat joint can significantly increase the shear capacity under dry joint conditions.

2.2.5 Adhesives

Zhou, Micklebrough, and Li (2005) found that the dry joints exhibited an average of 20-40% lower ultimate strength than that of epoxied joints. However, epoxy with a thickness that is 1 or 2 mm, has a higher shear strength than epoxy which is 3 mm thick. This suggested that using excessive epoxy would not help improve the shear strength of the joint but reduce the strength. Thus, using the appropriate amount of adhesive agent is important to make sure not carry a negative impact on the strength. Besides that, this paper also found that the epoxy actually can reduce the fitting imperfections at the joint and increases the rigidity of the segment as well as redistribute the shear load more evenly among the keys.

According to Ahmed and Aziz (2019), the ratio of the cracking load to the ultimate load for dry joints was ranging from 81-87%, whereas it was between 91 and 99% for epoxied joints. This also agreed that adding epoxy to joints can help in having improvement in the strength of the joints to withstand the shear loads. The finding in this study was well-aligned with that conducted by Zhou, Micklebrough, and Li (2005). Ahmed and Aziz (2019) also proposed that the application of epoxy can reduce joint imperfections and make it easier for shear forces to be distributed uniformly, which is also similar to the conclusions reached by Zhou, Micklebrough, and Li (2005).

In addition, the study by He et al. (2017) showed that different adhesion agents have variable degrees of effectiveness and may increase the strength of concrete interfaces to varying degrees. The investigation revealed that the mortar binders affect the most on the mechanical strength of the interface, which results in the most improvement of bond strength compared to other adhesives. Thus, the use of mortar binders will result in a stronger and more durable concrete structure, which has important consequences for the construction sector.

Moreover, Zhao et al. (2023) also concentrated on the impact of adhesives and interfacial roughness on the durability of the interface. The moulds were designed and created by the authors using 3D printing technology to achieve the desired interface shape. This study also discovered that using adhesives in conjunction with interfacial roughness was the best way to strengthen the interface. This result means that the adhesive used at the interface

can adjust the imperfections of the interface and behave like rubber to ensure that the shear stress can be effectively transmitted throughout the interface. This finding is similar to other research papers (Ahmed and Aziz, 2019; Zhou, Micklebrough, and Li, 2005).

In summary, it can be concluded that the use of an adhesive can improve the shear strength of the concrete interface. The mechanism of this adhesive is to reduce the imperfections in the joints and distribute the shear forces uniformly. However, the thickness of the adhesive used is critical as too much adhesive can adversely affect the interfacial strength. It is also concerned that the implication adhesive might surpass the contribution of the keyed joints to the overall shear strength.

2.2.6 Confining Pressure

Ayinde et al (2022), Wu, Ayinde and Zhou (2023) and Zhou, Micklebrough and Li (2005) also found that confining pressure can be considered as one of the parameters to investigate the influence of this aspect on the shear capacity of the concrete interface. Their results showed that the application of confining pressure can act as a further aid to improve the efficiency of the roughness tooth or key joint and has a significant positive effect on the interface shear capacity by improving the interface roughness.

Figure 2.5 shows an experimental result by Wu, Ayinde and Zhou (2023) on four specimens with different confining pressures such as 0MPa, 1MPa, 1.5MPa and 2MPa. The graph shows that the confining pressure provides the residual resistance for the interface after the primary failure (cracking) has occurred and increases the toughness of the interface as well as allowing a greater slip before ultimate failure. As a result, the shear strength of the concrete interface increases as the confining pressure increases.

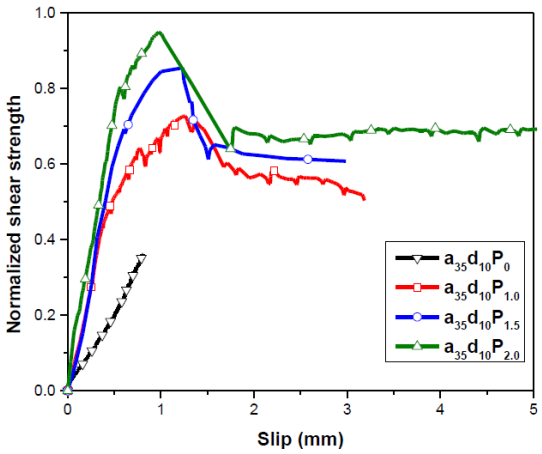

Figure 2.5: Normalised Shear Strength-Slip Curves of Four Specimens (Wu, Ayinde and Zhou, 2023).

Ayinde et al (2022) also carried out a study to investigate the effect of external pressure on the stress-slip curves. As shown in Figure 2.6, the initial stage of all three specimens with different external pressure shows a similar stress-slip relationship with a similar value. This indicates that increase in external pressure is not affect the initial stiffness, but the shear capacity of the interface increases as the external pressure increases. Moreover, an increase in external confining pressure results in an increase in residual stress, which is similar to the stress-slip curve obtained by Wu, Ayinde and Zhou (2023).

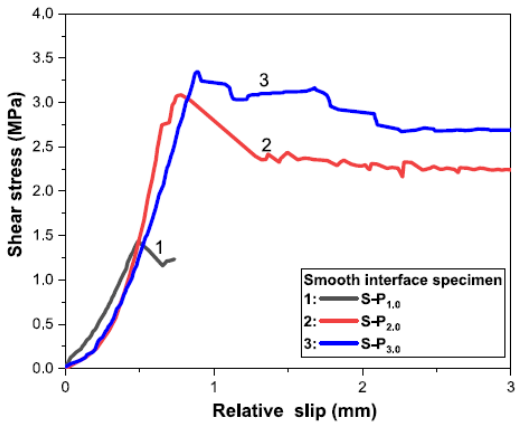

Figure 2.6: Shear Stress-Slip Curves for Smooth Interface Specimens (Ayinde et al., 2022).

Zhou, Micklebrough and Li (2005) also obtain a similar result that the normal stress can help to increase the normalised shear stress of the keyed joint. As shown in Figure 2.7, both types of keyed dry joints exhibit increasing shear capacity with increasing normal stress. This means that regardless of the condition of the interface, the normal stress can actually increase as the shear capacity of the interface by increasing the roughness of it.

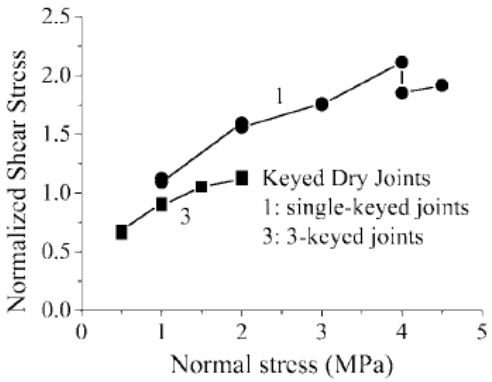

Figure 2.7: Graph of Normalised Shear Stress against Normal Stress of Keyed Dry Joints (Zhou, Micklebrough and Li, 2005).

Niwa et al. (2016) investigated the shear transfer at the interface of different aged concrete parts with different external prestressing forces. The study involved the reinforcement steel bar inside the concrete part to simulate the actual condition of the connection between new and old slabs. Figure 2.8 shows how the prestressing force act on the concrete by the green bar and the red bar represented the reinforcement.

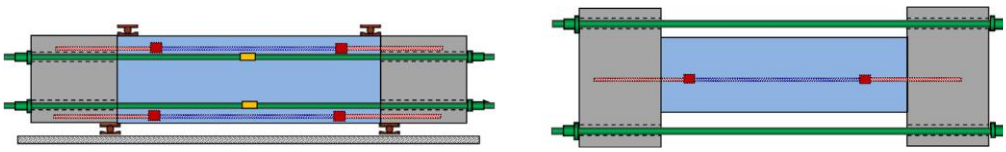

(a) Front View (b) Top View

Figure 2.8: Front and Top View of Specimen (a) Front View and (b) Top View (Niwa et al., 2016).

The authors found that the external prestressing forces increase the shear strength of the concrete, which agrees with the finding of Wu, Ayinde and

Zhou (2023) and Ayinde et al. (2022). As shown in Figure 2.9, the specimen with 2.0 MPa pressure can have the maximum shear capacity. Besides, this study also found that the failure pattern of the interface is strongly influenced by the initial prestressing level.

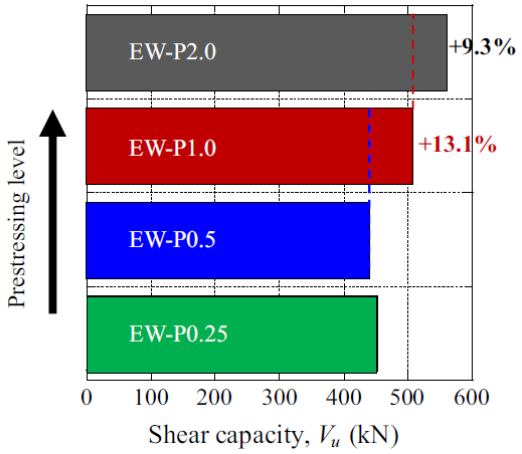

Figure 2.9: Shear Capacity under Different Prestressing Level (Niwa et al., 2016).

In short, the application of confining pressure can effectively increase the normal forces at the interface of the concrete, resulting in a greater surface friction. This increased roughness further increases the shear strength of the concrete interface. It can therefore be concluded that the use of confining pressure is a practical method of improving the mechanical properties, particularly the shear capacity, of concrete structures.

2.3 Failure Mode of Concrete Interface under Different Conditions

In order to properly understand the interface behaviour under shear loading, the crack pattern at the concrete interface is essential to assess the shear capacity and is an important step in determining the relationship between crack propagation and interface shear capacity. According to Niwa et al. (2016), the failure pattern at the interface can provide a certain level of estimation of the ultimate shear capacity. For example, the presence of a diagonal tensile crack on the specimen implies that the specimen has a higher ultimate shear capacity.

By monitoring the crack propagation, the type of failure and the location of the vulnerable part of the composite concrete can be identified. In

most case, the crack will normally occur at the concrete interface and propagate from the edge of the concrete part. Obtaining sufficient information on the relationship between the crack pattern and the shear behaviour can also assist in the calibration of the numerical simulation. By comparing the results of the numerical simulation, it can be ensured that the numerical model produced has a higher accuracy and reliability for analysing the shear behaviour of the concrete interface.

2.3.1 Key Joint

The cracking pattern of concrete was used as an idea for the shear behaviour in the experiment by Zhou, Micklebrough and Li (2005). The lower corner of the shear keys is often where the first crack appears, and it spreads at an angle of 45° to the horizontal. The shear zones then developed short diagonal cracks. When these two small diagonal cracks joined and reached the root of the key, the shear keys were sheared off. Figure 2.10 shows the crack progression for the single keyed dry and epoxy joints. Figure 2.11 and Figure 2.12 show the crack progression for the three-key dry and epoxy joints respectively.

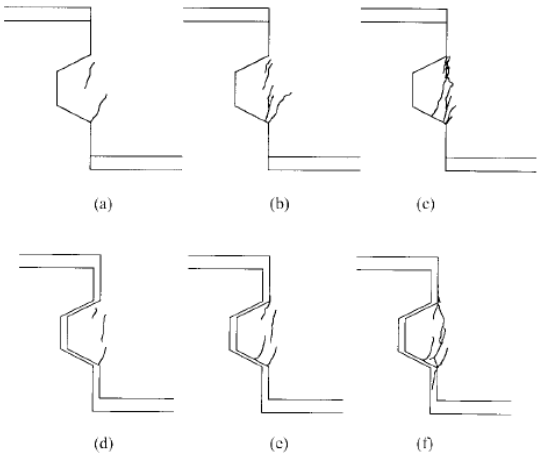

Figure 2.10: Crack Pattern for Single-Keyed Joints (Zhou, Micklebrough and Li, 2005).

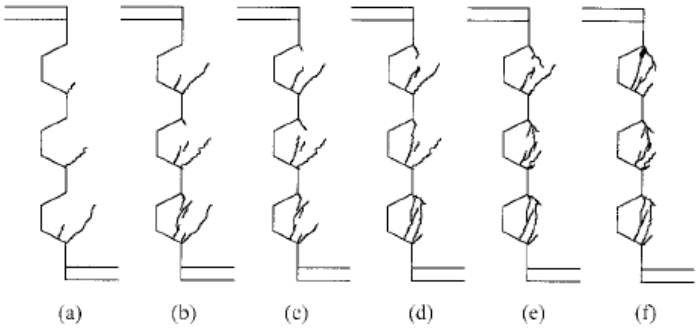

Figure 2.11: Crack Pattern for Three-Keyed Dry Joints (Zhou, Micklebrough and Li, 2005).

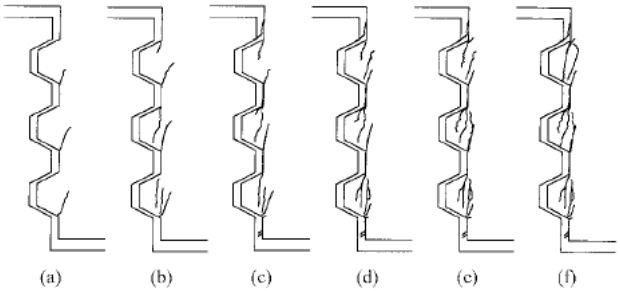

Figure 2.12: Crack Pattern for Three-Keyed Epoxied Joints (Zhou, Micklebrough and Li, 2005).

2.3.2 Confining Pressure

Niwa et al. (2016) identified three failure modes that occurred during the experiment: splitting, diagonal tension and mixed failure. The splitting failure occurs when the interface is smooth, and the reinforcement ratio is low. On the other hand, the diagonal tension failure occurs when the interface is rough, and the reinforcement ratio is high. Mixed failure occurs when the interface is rough, and the reinforcement ratio is moderate.

The main finding of this study is that the diagonal tension crack has a significant effect on the shear strength of the interface as it compresses the upper fibre of the interface. This means that the shear load has been transferred to the other section to relieve the shear stress in the interface region. This results in an increased shear capacity. The different crack patterns that occur on the specimen are shown in Figure 2.13.

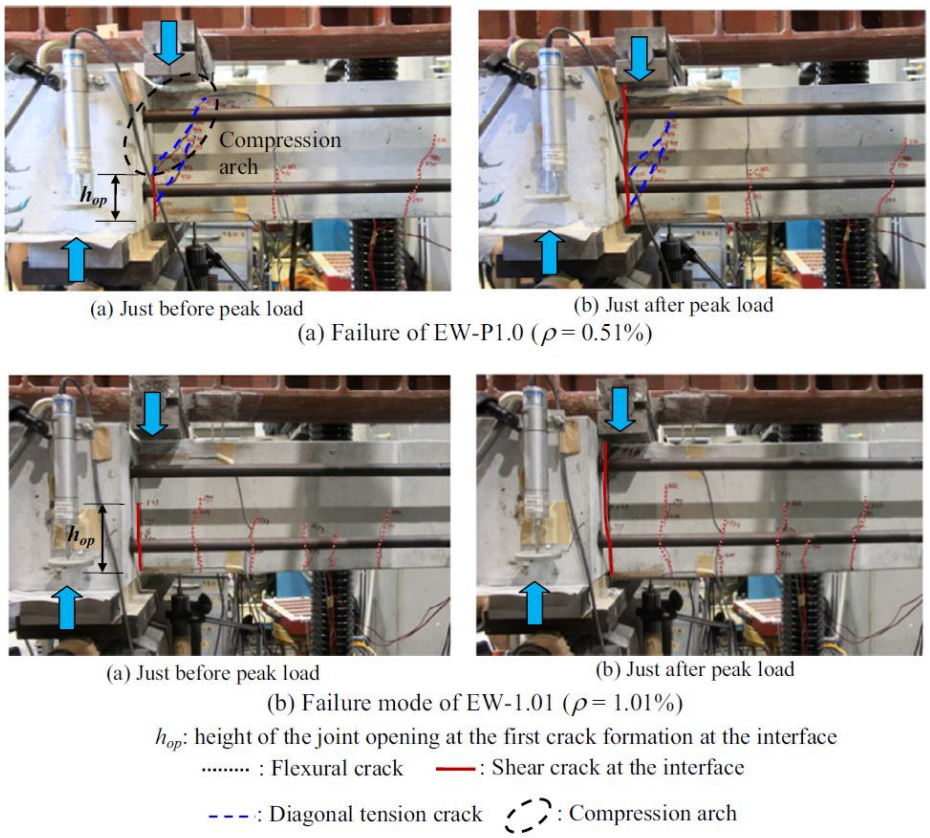

Figure 2.13: Crack Pattern of Specimens (Niwa et al., 2016).

While at a later time, Wu, Ayinde and Zhou (2022) conducted a similar experiment in term of concrete interface with grooved surface. The results of Wu, Ayinde and Zhou (2022) showed that there are two failure modes of the specimens, which are the adhesive failure mode and the cohesive failure mode. The adhesive failure mode is due to the separation of the interface. This failure mode was observed when the shear stress at the interface exceeded the bond strength between the two layers. The cohesive failure mode was due to the crushing of the interface roughness tooth. This failure mode was observed when the shear stress experienced by the concrete interface exceeded the shear capacity of the roughness tooth. Figure 2.14 shows the failure mode of the concrete specimen.

Figure 2.14: Failure Mode of Concrete Interface with Grooved Surface (Wu, Ayinde and Zhou, 2022).

However, no visible diagonal tension cracks were observed in the specimen throughout the experiment. This finding was different from that of Niwa et al. (2016), who obtained diagonal tension cracks and increased shear strength. The authors stated that the possible reason for this difference could be due to the reduced load eccentricity maintained in the experimental configuration of Wu, Ayinde and Zhou (2022), as opposed to the larger load eccentricity observed in the study of Niwa et al. (2016). Besides that, Niwa et al. (2016) stated that the diagonal tensile failure occurs when the interface is rough, and the reinforcement ratio is high. Thus, the direction of crack propagation may be different because the reinforcement is considered in the study of Niwa et al. (2016), but the specimens in the study of Wu, Ayinde and Zhou (2022) did not have any reinforcing fibres inside.

Recently, Wu, Ayinde and Zhou (2023) carried out the experiment using a similar test setup to Wu, Ayinde and Zhou (2022) in terms of single triangular roughness tooth. The results of Wu, Ayinde and Zhou (2023) showed that the specimens tested during the experiment also exhibited either cohesive or adhesive failure behaviour. The failure of the concrete specimen is shown in Figure 2.15. The results of this study provide a general understanding of how the concrete interface responds to shear loading and how cracking occurs under confining pressure.

(a) Interface failure (b) Shear failure of the roughness tooth

Figure 2.15: Typical Failure of Double Shear Test Specimen (Wu, Ayinde and Zhou, 2023).

If the specimen obtained the adhesive failure, which means that the shear load is concentrated on the interface and the shear load is not carried by the roughness tooth. However, if the specimen obtained the cohesive failure, it means that the shear load is carried by the roughness tooth and the shear capacity will mainly depend on the strength of the tooth. This emphasises that the effectiveness of the tooth is highly dependent on the size of the tooth when under confining pressure.

In addition, the specimen without confining pressure showed pure adhesive failure at the contact. When failure occurred at the contact, the specimen parts separated, and the test was terminated as the specimen failed completely with no residual resistance. However, in the 1.0 MPa specimen, the confinement system provides confining pressure on the specimen to keep the parts in contact after cracking has occurred. According to Wu, Ayinde and Zhou (2023), due to the presence of confining pressure, the shear crack started at the root of the tooth and propagated diagonally. This propagation path is identical to the fracture direction determined by Zhou, Micklebrough and Li (2005).

2.4 Finite Element Method (FEM)

According to Kuna (2013), FEM is a numerical technique that can transform partial differential equations into a matrix equation for their solution. FEM allows the use of Galerkin techniques to estimate partial differential equations, as well as the interpolation of functions or vector fields in multidimensional domains. In addition, FEM also allows the efficient implementation of low-order and isoparametric approaches for both stationary and evolutionary model problems (Bartels, 2016). In recent years, a number of different studies (Wu,

Ayinde and Zhou, 2023; Shamass, Zhou and Alfano, 2015; Ayinde et al., 2022) have been carried out to investigate the shear behaviour of concrete interfaces under different conditions using FEM.

FEM is a powerful tool for simulating the behaviour of concrete specimens. It eliminates the need for physical casting and the lengthy 28-day strength development, significantly reducing testing time. Besides that, FEM allows rapid estimation of results for various parameters, including concrete strength, geometry and surface properties. As shown by Wu, Ayinde and Zhou (2023), FEM can simulate various factors such as roughness angles, depths, number of tooth and pressures. While FEM is fast and efficient, physical testing remains important for validation. This is because simulations often assume an ideal environment, neglecting the complexities and potential inconsistencies of the real world. Therefore, combining the FEM with empirical validation can help to achieve an accurate result.

2.4.1 Comparison between Numerical Results and Experimental Results

Wu, Ayinde and Zhou (2023) used the CDP model to simulate the response of the interface under shear stress. Figure 2.16 shows that their simulation closely follows the experimental data in the elastic phases. However, there are still small discrepancies in the inelastic phase at the test specimen with confining pressure. These discrepancies are probably due to slight misalignments in the contact between the plates and specimens during the experiment. In contrast, the finite element simulation assumes perfect contact conditions. Despite these misalignments, the simulated results remain in close agreement with the experimental data, with the ratio of simulated to experimental values ranging from 0.99 to 1.09. This indicates that the CDP model effectively captures the real behaviour of the concrete interface under shear loading.

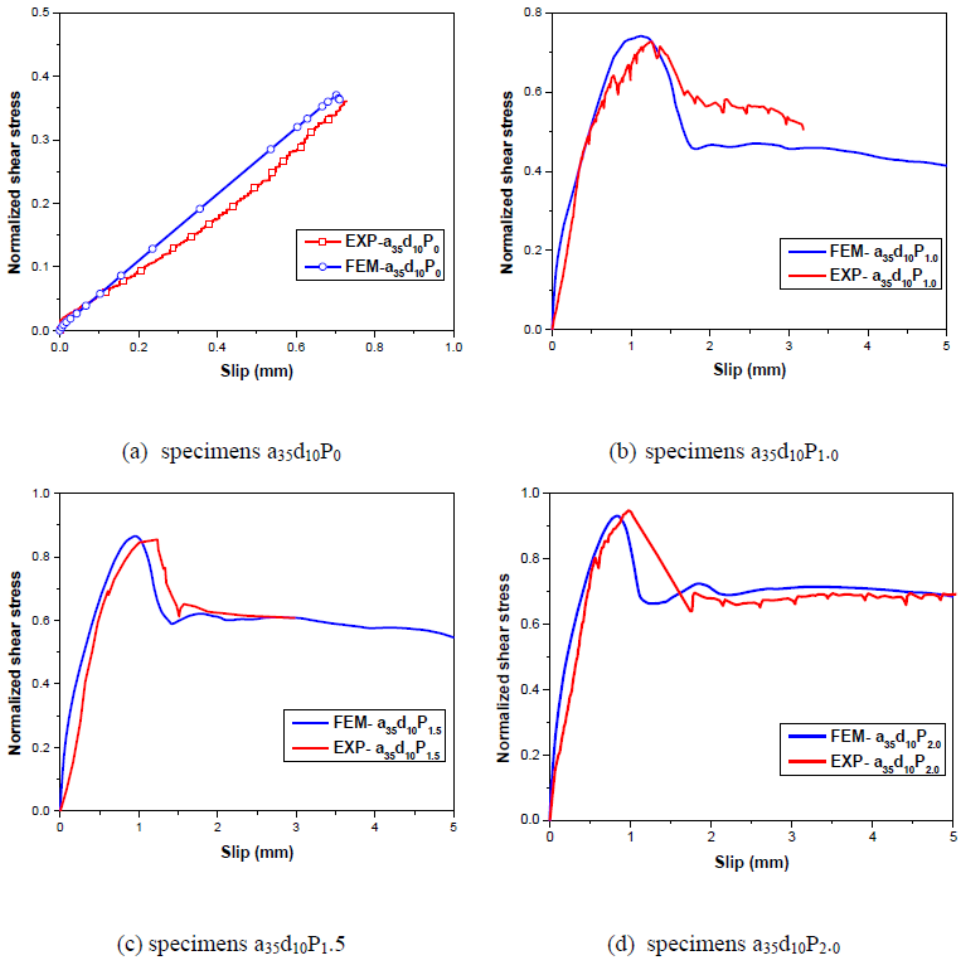

(a) specimens $a_{35}d_{10}P_0$ (b) specimens $a_{35}d_{10}P_{1.0}$

(c) specimens $a_{35}d_{10}P_{1.5}$ (d) specimens $a_{35}d_{10}P_{2.0}$

Figure 2.16: Comparison between Experimental Results and Numerical Results (Wu, Ayinde and Zhou, 2023).

2.4.2 Effect of Concrete Strength and Confining Pressure on Keyed Dry Joints

Shamass, Zhou, and Alfano (2015) developed a CDP model by incorporating insights from previous studies on the effects of confining pressure (Buyukozturk et al., 1990) and concrete strength (Zhou et al., 2005). Figure 2.17 illustrates the finite element model extracted from both studies and used for the analysis.

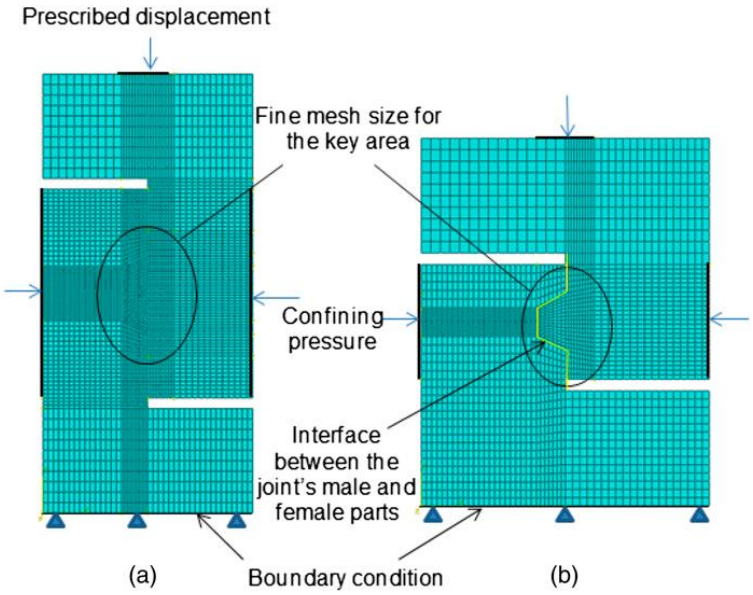

Figure 2.17: Finite Element Mesh of Models (a) Buyukozturk et al. (1990) (b) Zhou et al. (2005) (Shamass, Zhou and Alfano, 2015).

The model accurately predicted the shear strength values, with an average deviation from the experimental results of only 9%, and this small difference guarantees the reliability of the model. The load-deflection curves shown in Figure 2.18 and Figure 2.19 show a significant drop at peak strength, indicating shear failure of the key.

Additionally, the results showed that both ultimate and residual shear strength increased with higher concrete strength and confining pressure. Even after failure, residual strength persisted due to confinement between cracked concrete surfaces. Figure 2.19 highlights the significant influence of confining pressure on residual strength, with higher pressure resulting in increased initial stiffness and peak load displacement.

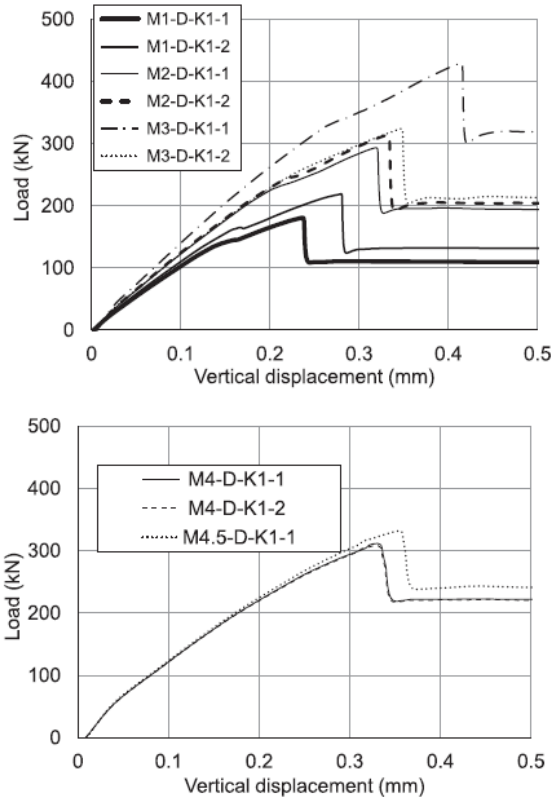

Figure 2.18: Effect of Concrete Strength on Keyed Dry Joint Performance of Zhou et al. (2005) (Shamass, Zhou and Alfano, 2015).

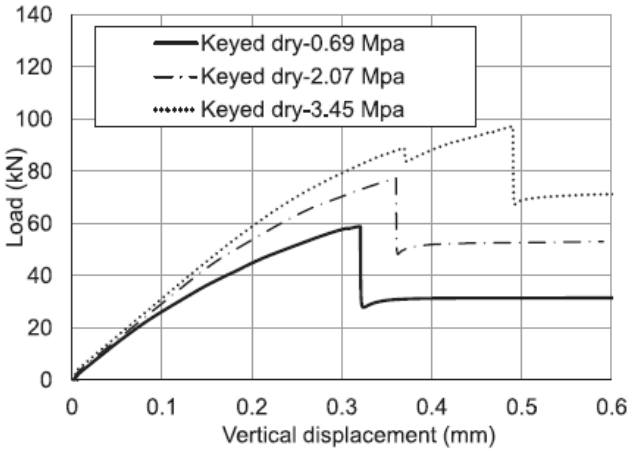

Figure 2.19: Effect of Confining Stress on Keyed Dry Joint Performance of Buyukozturk et al. (1990) (Shamass, Zhou and Alfano, 2015).

Figure 2.20 shows how increasing the confining pressure can reduce the length of the bottom key crack (S crack) in single-keyed dry joints. The S

crack occurs when the lower key surface carries most of the shear load. At 6 MPa confining pressure, the S crack disappears entirely. This is because the formation of a high compression zone under higher pressure will stop the inclined cracks and confine existing vertical cracks within this zone.

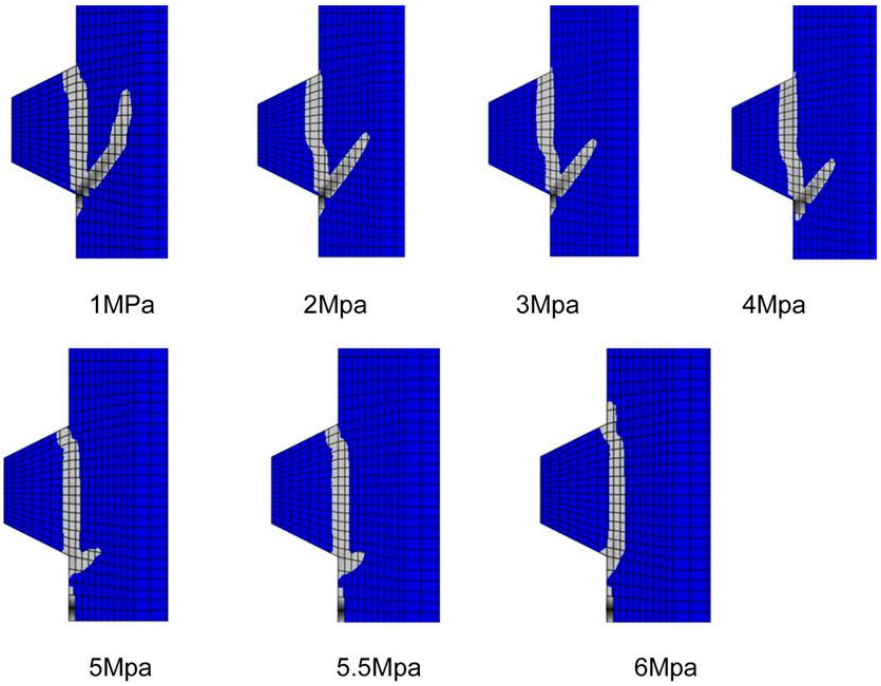

Figure 2.20: Crack Pattern of Key-joint under Different Magnitude of Confining Pressure (Shamass, Zhou and Alfano, 2015).

2.4.3 Effect of Roughness Tooth Angle

Wu et al. (2023) and Ayinde et al. (2022) investigated the influence of varying roughness tooth angle on the shear behaviour of concrete interfaces. Both studies used a “Hard” contact model with friction penalty, but Wu, Ayinde and Zhou (2023) also included cohesive behaviour to simulate the cold joint formed between new and old concrete. This difference in modelling approach led to contrasting results.

Figure 2.21 compares the results of both studies using specimens with roughness angles ranging from 10° to 50°. Ayinde et al (2022) observed a consistent stiffness across all angles, suggesting a minimal effect of roughness on this parameter. Conversely, Wu et al (2023) found an increase in initial stiffness from 10° to 35°, followed by a decrease until 50°.

This discrepancy is due to the different interface models used. While both studies used the “Hard” contact model, the inclusion of cohesive behaviour by Wu et al. (2023) provides a more realistic representation of the actual interface. Concrete interfaces, particularly cold joints, exhibit cohesive behaviour due to the bond between new and old concrete. Inclusion of this element is critical to accurately capture the interface response.

Despite the difference in stiffness results, both models showed similar trends in the overall relationship between shear resistance and slip. However, by taking into account the cohesive interaction of concrete interfaces, Wu et al. (2023) model is able to provide a more accurate representation of the actual behaviour.

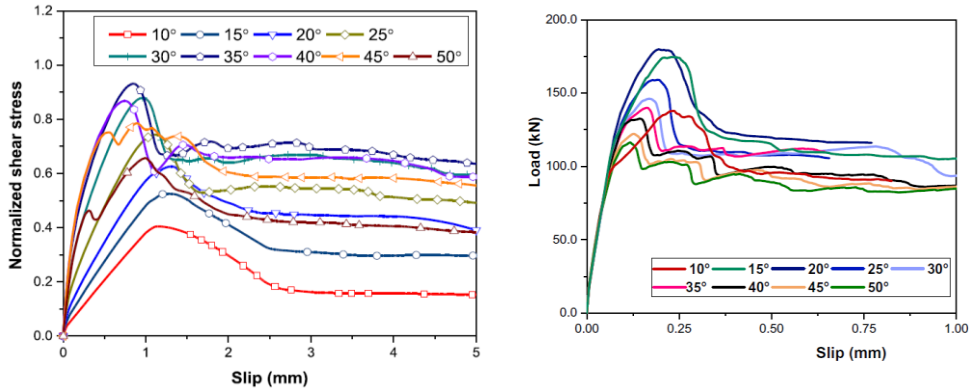

(a) Wu, Ayinde and Zhou (2023) (b) Ayinde et al. (2022)

Figure 2.21: Stress-Slip Curves with Varying Tooth Angles (a) Wu, Ayinde and Zhou (2023) and (b) Ayinde et al. (2022).

In addition, the different modelling approach used in the two studies has led to differences in their findings regarding the optimum tooth angle. Wu, Ayinde and Zhou (2023) found a polynomial relationship between tooth angle and interfacial strength, suggesting an optimum angle of about 35° to maximise shear strength in simulations as shown in Figure 2.22(a). However, Ayinde et al. (2022) found a similar trend, but with an optimum angle of 20°.

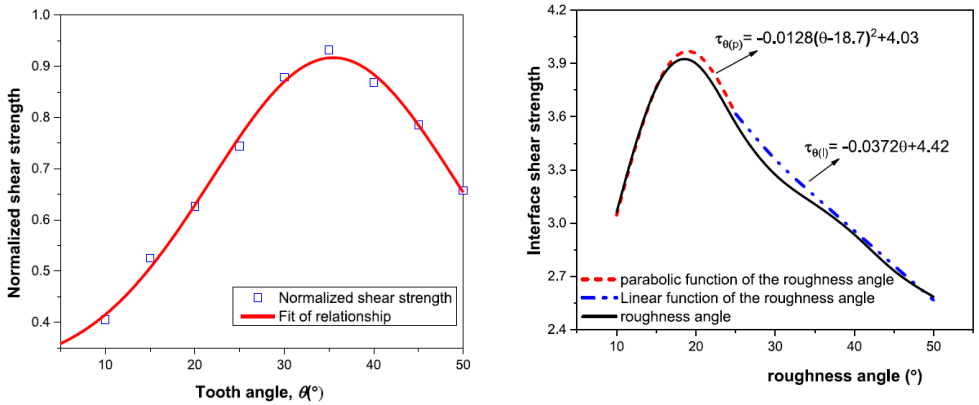

(a) Wu, Ayinde and Zhou (2023) (b) Ayinde et al. (2022)

Figure 2.22: Shear Strength and Tooth Angle Relationship Curves (a) Wu, Ayinde and Zhou (2023) and (b) Ayinde et al. (2022).

Figure 2.23 demonstrates this capability by showing the failure modes of the specimens obtained by Wu, Ayinde and Zhou (2023). Two main crack patterns are observed which are diagonal tension cracks and a combination of diagonal tension cracks with shear cracks. Diagonal tension cracks occurred only at lower tooth angles (10°-20°), indicating the absence of roughness tooth failure. This suggests that the interface shear strength was primarily dependent on the bond between the old and new concrete. Diagonal tension cracks with shear cracks occurred at higher tooth angles (25°-50°), which is considered the ideal response to shear loading, as reported by Niwa et al. (2016) and Shamass, Zhou and Alfano (2015).

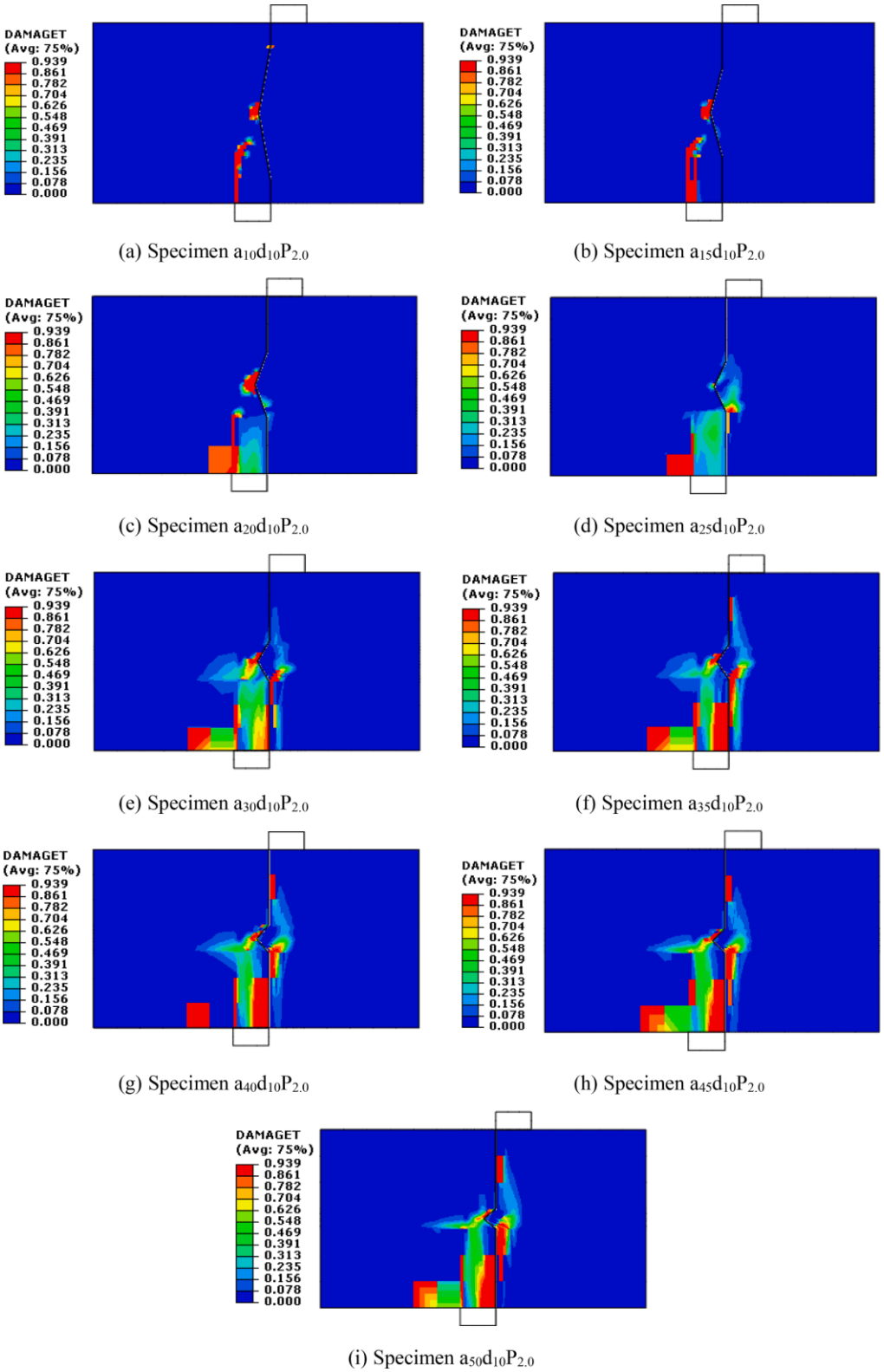

(a) Specimen $a_{10}d_{10}P_{2.0}$ (b) Specimen $a_{15}d_{10}P_{2.0}$

(c) Specimen $a_{20}d_{10}P_{2.0}$ (d) Specimen $a_{25}d_{10}P_{2.0}$

(e) Specimen $a_{30}d_{10}P_{2.0}$ (f) Specimen $a_{35}d_{10}P_{2.0}$

(g) Specimen $a_{40}d_{10}P_{2.0}$ (h) Specimen $a_{45}d_{10}P_{2.0}$

(i) Specimen $a_{50}d_{10}P_{2.0}$

Figure 2.23: Numerical Simulated DamageT Contour with Varying Tooth Angle (Wu, Ayinde and Zhou, 2023).

2.4.4 Effect of Roughness Tooth Depth

Previous researches (Wu, Ayinde and Zhou, 2023; Ayinde et al., 2022) have investigated the effect of varying tooth depth on the shear behaviour of concrete interfaces. Figure 2.24 summarises their findings. The results showed that the overall shape of the stress-slip curve remained unaffected, while tooth depth significantly influenced the shear capacity.

Ayinde et al (2022) used tooth depths of 5-15 mm while Wu, Ayinde and Zhou (2023) used a wider range of 5-50 mm. This wider range in the latter study provides a more comprehensive picture. Wu, Ayinde and Zhou (2023) found that the initial interface stiffness increased with increasing tooth depth. Shear strength also showed a significant increase of 87% as tooth depth increased from 5 mm to 35 mm. However, further increases showed no significant increase, suggesting an optimum depth of 35 mm to maximise shear capacity.

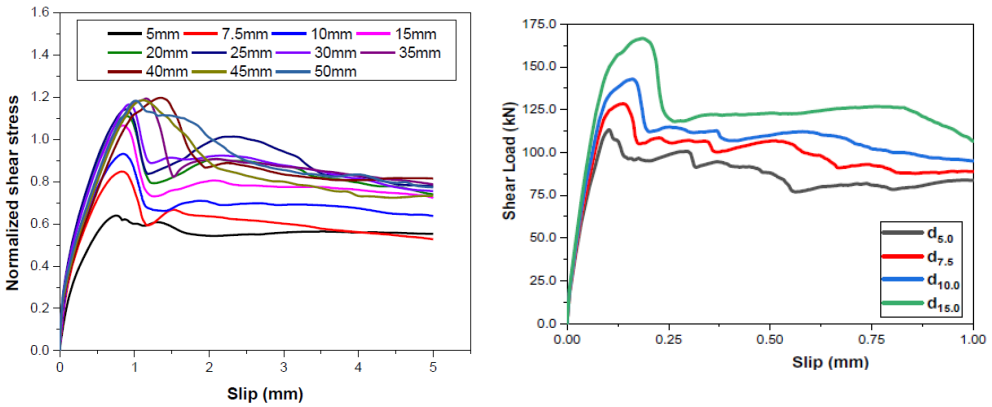

(a) Wu, Ayinde and Zhou (2023) (b) Ayinde et al. (2022)

Figure 2.24: Shear Slip Curves with Varying Tooth Depth (a) Wu, Ayinde and Zhou (2023) and (b) Ayinde et al. (2022).

Figure 2.25 shows the relationship between shear strength and tooth depth at a constant confining pressure. The limited range of the previous study is evident here as their results diverge: Wu, Ayinde and Zhou (2023) found a positive effect on shear strength up to 35 mm, while Ayinde et al. (2022) found a linear relationship. The use of specimens with a wider range of tooth depths would provide a clearer relationship and help to understand the mechanisms operating in the interface region.

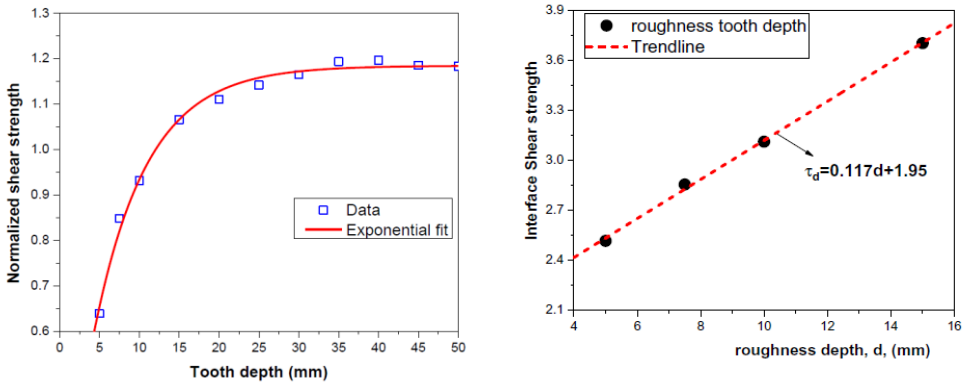

(a) Wu, Ayinde and Zhou (2023) (b) Ayinde et al. (2022)

Figure 2.25: Shear Strength and Tooth Depth Relationship Curves (a) Wu, Ayinde and Zhou (2023) and (b) Ayinde et al. (2022).

Figure 2.26 shows simulated crack patterns in concrete interfaces with varying tooth depths. As the depth increases, the length of S-cracks that form at the root of the roughness tooth in the new concrete section increases. This suggests that the new concrete parts and the upper key layer are carrying a greater load, similar to the findings of Shamass et al. (2015). This implies that roughness tooth failure consistently initiates at the base corner.

Besides that, this crack propagation indicates that after interface bond failure, the shear strength of the interface is primarily dependent on the shear strength of the roughness tooth. In particular, the S-cracks disappeared at 35 mm tooth depth and decreased steadily until they were completely absent at 50 mm. In this case, the cracks occur mainly in the roughness tooth tip of the new concrete.

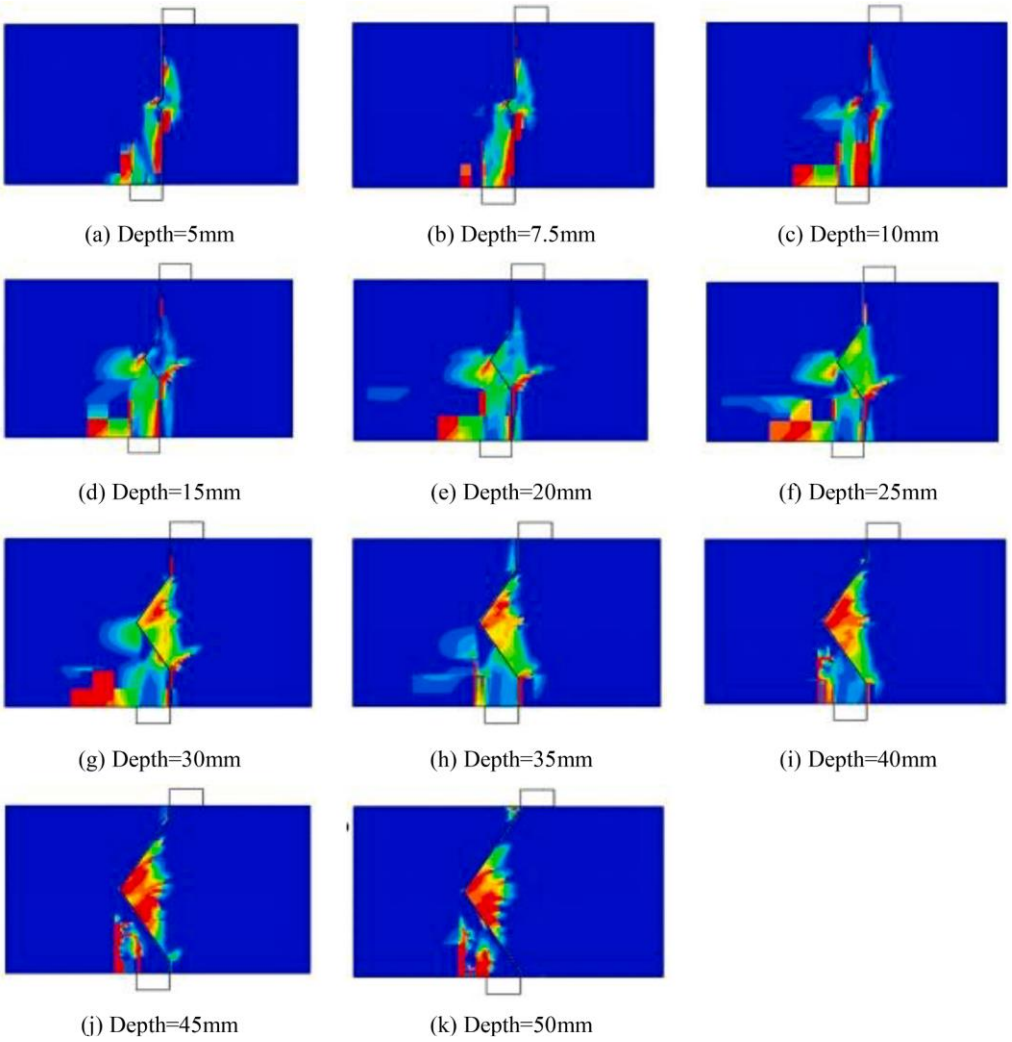

Figure 2.26: Numerical Simulated DamageT Contour with Varying Tooth Depth (Wu, Ayinde and Zhou, 2023).

However, both studies did not investigate the effect of load eccentricity (from the loading plate and base support) on the optimum tooth depth. With reference to the simulated crack pattern that having various depth, the result of varying roughness tooth depth might also be affected by the width of the top plate and bottom plate, as the eccentricity of the shear load might affect the shear load transfer mechanism at the interface. Therefore, further research is required to determine the optimum depth for different load conditions.

2.5 Summary

Several factors have been identified that can influence the behaviour of the concrete joint between two differently aged members. Wu, Ayinde and Zhou (2022, 2023) found that the normalised shear strength of the concrete interface

is strongly influenced by the tooth angle. Wu, Ayinde and Zhou (2023) suggested that the single triangular tooth angle should ideally be 35° and that exceeding this angle may result in reduced strength.

The interfacial shear strength is also influenced by the roughness depth or fractal dimension, as highlighted by He et al. (2017), Ayinde et al. (2022) and Wu, Ayinde and Zhou (2022, 2023). In addition, according to Yuan et al. (2021), the incorporation of fibres into concrete can improve the bond strength of the concrete interface.

The combination of key joint and adhesive is the main factor influencing the shear behaviour of the concrete interface, as it helps to reduce fitting imperfections and improve segment stiffness, as well as distributing the shear load evenly across the keys. Zhou, Micklebrough, and Li (2005), Ahmed and Aziz (2019), and Zhao et al. (2023) have highlighted the role of adhesives in achieving fitting imperfections between two concrete members. He et al. (2017) has shown that the incorporation of mortar binders can lead to stronger and more durable concrete structures.

The confining pressure is also an important parameter to consider when investigating the shear capacity of composite concrete, as shown by Wu, Ayinde, and Zhou (2022, 2023), Zhou, Micklebrough, and Li (2005), and Niwa et al. (2016). The confining pressure can prevent the interface from separating after the failure of the interfacial bond, and aid in load transfer. The shear strength of a specimen increases with increasing confining pressure.

Wu, Ayinde, and Zhou (2023) found that the specimens tested in their experiment exhibited either cohesive or combination of cohesive and adhesive failure mode. However, Niwa et al. (2016) found three failure modes in their experiment, including cleavage, diagonal tension, and mixed failure.

Numerous studies (Wu, Ayinde and Zhou, 2023; Shamass, Zhou and Alfano, 2015; Ayinde et al., 2022) have demonstrated the validity of numerical techniques to simulate the shear behaviour of concrete interfaces and the simulation results have shown good agreement with experimental results. These studies have also shown that the nonlinear analysis programme can be used to investigate the shear behaviour of concrete interfaces under a wide range of conditions such as different concrete strengths, confining pressures, triangular roughness tooth depths and angles.

However, it is noteworthy that a comprehensive investigation on the effect of a rectangular roughness tooth on the shear behaviour of concrete interface has not been conducted as the previously mentioned studies were not considered on this topic. Despite the exploration of various factors like tooth angles, adhesive properties, confining pressures, and other parameters, none of them has specifically dealt with how the introduction of rectangular roughness tooth may affect the behaviour of the concrete interface.

CHAPTER 3

METHODOLOGY

3.1 Introduction

The aim of this research was to investigate the effectiveness of rectangular roughness tooth in improving the shear behaviour of the concrete interface. While previous studies have investigated other roughness methods, the effect of rectangular shapes has not been investigated.

To achieve the objectives of this study, ABAQUS software was used to simulate and visualise the behaviour of the concrete interface under shear loading. This software allows the observation, analysis and prediction of various aspects including cracking, deformation and the relationship between applied shear stress and interface slip.

Before starting the simulation process, it is necessary to define the specimen specifications. This involves determining the size and strength of the concrete specimens, as well as the loading conditions. The first objective of the study is to develop an accurate numerical model that closely replicates the behaviour observed in actual double shear tests.

Therefore, where there are discrepancies between the numerical and experimental results, a calibration process has been carried out. This involves iteratively refining the model parameters until the numerical results closely match the observed experimental data. Once the model is calibrated, key parameters such as interface stiffness, interface failure initiation and damage evolution are extracted and incorporated into the test specimen models for further analysis.

The numerical analyses were performed on specimens with different tooth parameters and confining pressure conditions. This analysis allowed the acquisition and recording of the predicted failure mode, crack patterns and normalised shear strength of the specimens as the parameters from reference specimen models keyed into the numerical model. The relationship between the tooth thickness of the rectangular roughness tooth and the application of confining pressure and the overall shear behaviour of the concrete interface was then identified. The overall process of this study is shown in Figure 3.1.

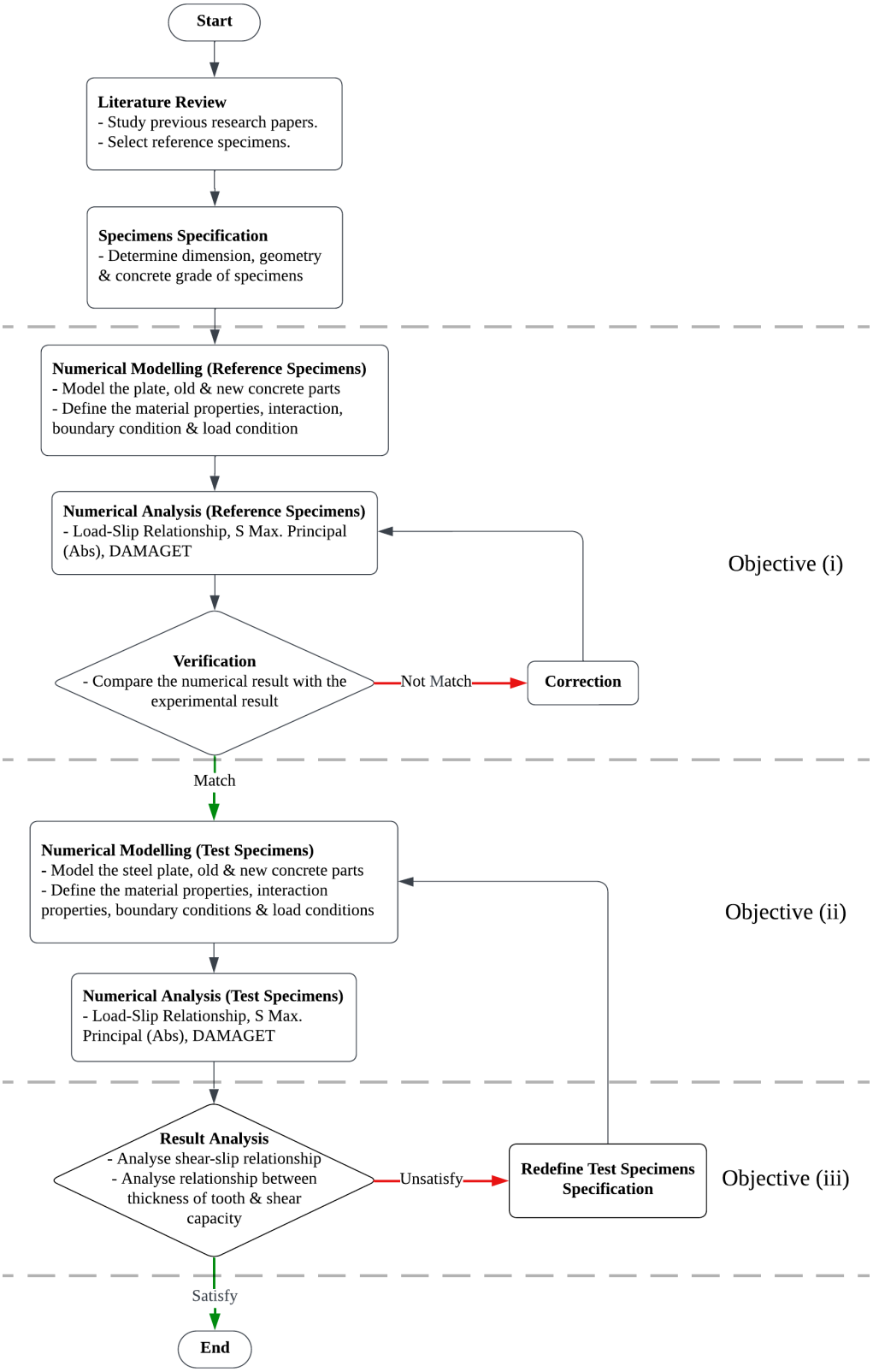

Figure 3.1: Flowchart of Study.

3.2 Review on Historical Study

The research of Wu, Ayinde and Zhou (2023) has been used as a reference in this numerical investigation. The test used by the authors to investigate the concrete interface is the double shear test. Figure 3.2 shows the configuration of the double shear test. The load cell was placed above the distribution beam to capture the total shear load applied to the specimen and two linear variable differential transducers (LVDT) were placed beneath the specimen to capture the slip. The model output followed the exact test setup to ensure a consistent data acquisition method and to avoid any unwanted inconsistencies. In addition, the overall specification such as geometry and dimensions of the specimen was also used as a standard to follow, but the geometry of the roughness tooth of the test specimens was modified to suit the aim and purpose of this study.

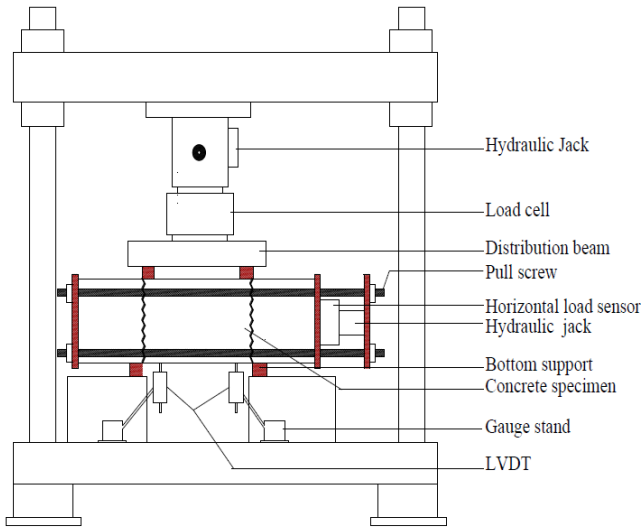

Figure 3.2: Test Setup (Wu, Ayinde and Zhou, 2023).

3.3 Specimen Specification

Specification of the specimen is very important as the specimen geometry, specimen size and location of the roughness tooth can be significant parameters that influence the simulation result for the numerical study. In this study, there were two types of specimens, the reference specimens and the test specimens. In this study, each type will serve a specific purpose and has been explained in detail in the following subsection.

3.3.1 Reference Specimens

The reference specimens were used as a benchmark for the specification of the test specimens. The parameters of the test specimens such as geometry, dimensions, concrete grade and also interaction properties are determined based on the reference specimens. The reference specimens used in this research correspond to the specimens described in the research report by Wu, Ayinde and Zhou (2023). The experimental data for the reference specimens was also used to fine-tune the numerical model in this study.

The reference specimens consist of a new concrete measuring 250 mm × 150 mm × 150 mm and two old concretes, each measuring 150 mm × 150 mm × 150 mm. At the centre of the interface, there is a triangular roughness tooth with a depth of 10 mm and a triangular roughness angle of 35°. The compressive strengths used by the authors for the old and new concretes were 28.0 MPa and 43.0 MPa respectively. Table 3.1 shows the specification of the reference specimen without confining pressure, while Table 3.2 shows the specification of the reference specimen with 1.0 MPa confining pressure. Figure 3.3 shows a schematic side view of the reference specimens as a visual aid.

Table 3.1: Reference Specimen 1 (R01) Specification.

Parameter	**Description**
Annotation	R01
Dimension	550 mm (Length) x 150 mm (Width) x 150 mm (Height)
Roughness Tooth Shape	Triangle
Roughness Tooth Specification	Depth = 10 mm Angle = 35°
Confining Pressure	0 MPa
Concrete Strength	28 MPa (Old Concrete) & 43 MPa (New Concrete)

Table 3.2: Reference Specimen 2 (R02) Specification.

Parameter	Description
Annotation	R02
Dimension	550 mm (Length) x 150 mm (Width) x 150 mm (Height)
Roughness Tooth Shape	Triangle
Roughness Tooth Specification	Depth = 10 mm Angle = 35°
Confining Pressure	1.0 MPa
Concrete Strength	28 MPa (Old Concrete) & 43 MPa (New Concrete)

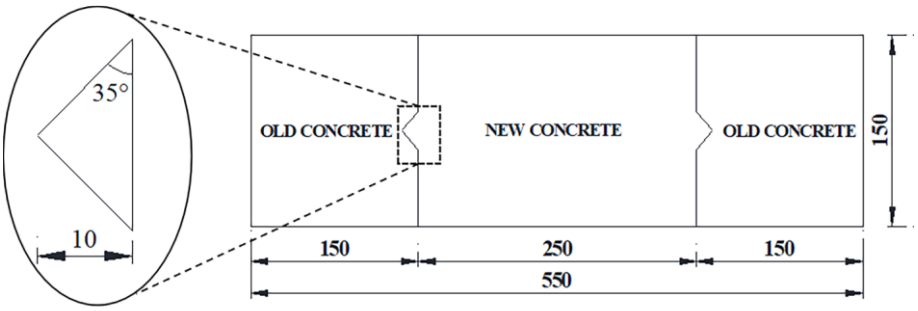

Figure 3.3: Detailing of Reference Specimen (Wu, Ayinde, and Zhou, 2023).

The physical experimental test results were extracted and used in this study to calibrate the numerical models. In cases where discrepancies were found between these results, an iterative recalibration process was carried out by adjusting the parameters of the interaction properties between the concrete parts until the numerical output matched the experimental data. Both the stress-strain curves corresponding to the specimen without confining pressure and 1.0 MPa were used as experimental data in this investigation. The results of the load-slip curve extracted from the study are shown in Figure 3.4.

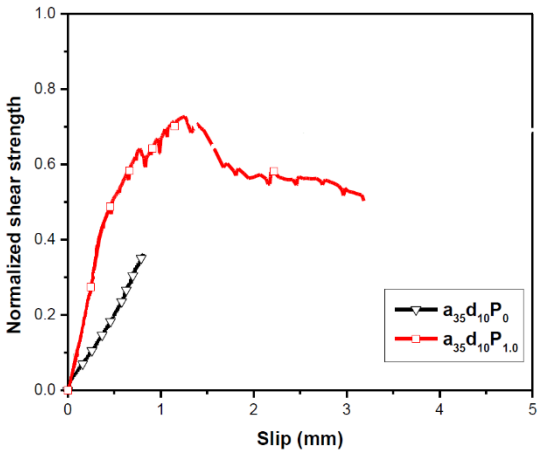

Figure 3.4: Normalised Shear Stress-Slip Curves ($a_{35}d_{10}P_0$ and $a_{35}d_{10}P_{1.0}$ Represent the Reference Specimen R01 and R02 respectively) (Wu, Ayinde, and Zhou, 2023).

Furthermore, the two failure modes obtained by Wu, Ayinde and Zhou (2023) were also used as a reference to compare with the result of the numerical model. Figure 3.5 shows two types of failure obtained by the authors, which are adhesive failure (debonding at the interface) and cohesive failure (failure at the roughness tooth). In their case, the adhesive failure occurred on the specimen without confining pressure while the combination of adhesive and cohesive failure occurred on the specimen with confining pressure.

(a) Interface failure (b) Shear failure of the roughness tooth

Figure 3.5: Types of Failure (Wu, Ayinde, and Zhou, 2023).

3.3.2 Test Specimens

The test specimens used in this study have the same overall dimensions, concrete grade, and geometry as the reference specimens. However, the difference between the test specimens and the reference specimens was that the test specimens had a rectangular roughness tooth in the centre of the concrete

interface instead of a triangular tooth. In this study, the thickness of the rectangular tooth was varied to assess its influence while keeping the depth of the tooth constant. The depth of the rectangular roughness tooth remained fixed at 10 mm as the depth of the reference specimens was also 10 mm to avoid extrapolation of the result which could make the numerical result unreliable.

This study investigated not only the geometric parameter but also the influence of the confining pressure on the effectiveness of the rectangular tooth. To investigate variations in tooth thickness and the presence of confining pressure, two batches of models were created and simulated. Batch A was the specimens without confining pressure, while the Batch B was the specimens subjected to 1.0 MPa confining pressure. Each batch had nine different tooth thicknesses which were ranging from 30 mm to 70 mm. Table 3.3 shows the specifications of the two batches of specimens used in this study. The specimen identification scheme used in this study was referred to as *Ti-j*. The symbol "T" stands for test specimens, "*i*" is the confining pressure value in MPa for the specimens and "*j*" is the roughness tooth thickness in mm. All specimen details for both batches are shown in Figure 3.6.

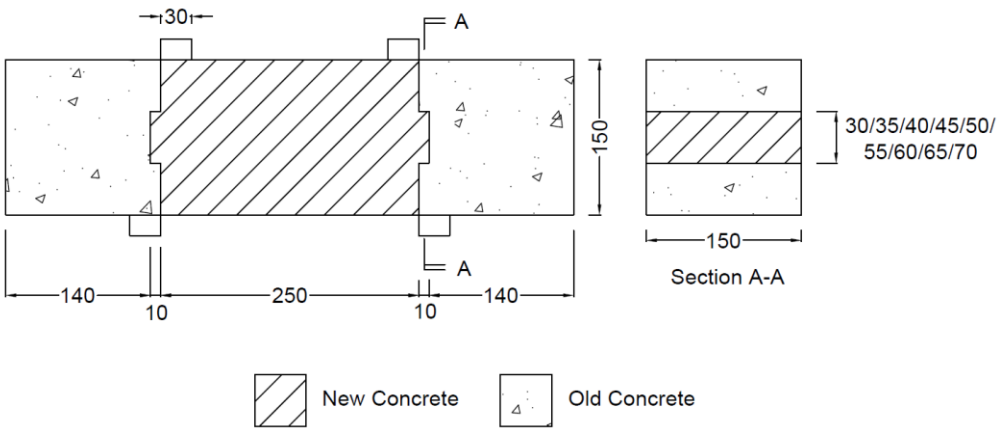

Figure 3.6: Test Specimens Drawing.

Table 3.3: Test Specimens Specification

Specimen	Roughness Tooth Thickness (mm)	Specimen	Roughness Tooth Thickness (mm)
Batch A: 0 MPa Confining Pressure			
T0-30	30	**T0-55**	55
T0-35	35	**T0-60**	60
T0-40	40	**T0-65**	65
T0-45	45	**T0-70**	70
T0-50	50		
Batch B: 1.0 MPa Confining Pressure			
T1-30	30	**T1-55**	55
T1-35	35	**T1-60**	60
T1-40	40	**T1-65**	65
T1-45	45	**T1-70**	70
T1-50	50		

3.4 Finite Element Modelling

This investigation was carried out using ABAQUS to assist in obtaining the numerical result of the test specimens in order to study the effect of various parameters of the rectangular roughness tooth on the shear behaviour of the concrete interface. The Concrete Damage Plasticity (CDP) model is a numerical model provided by ABAQUS for simulating the response and behaviour of concrete structures under various loading and compression conditions in terms of plastic damage. This model is widely used to simulate and estimate the damage behaviour and non-linear deformation characteristics of concrete.

The CDP model represents the inelastic behaviour of concrete by combining the isotropic damaged elasticity combined with isotropic tensile and compressive plasticity (Dassault Systemes, 2019). Besides that, the CDP model is based on the scalar (isotropic) damage assumption and is intended for situations where the concrete is subjected to random loading conditions, such as cyclic loading. The model also accounts for the plastic strain induced deterioration of elastic stiffness in both tension and compression.

The model consisted of three separate components: old concrete, new concrete and steel plate. Both concrete parts were modelled as 3D deformable solids, while the steel plate was modelled as a 3D rigid analytical shell. This approach was chosen because the deformation of the steel plate is not relevant to the analysis and the results focus only on the behaviour of the concrete specimen.

Once the component modelling was complete, there were four stages to the model definition process, including material property definition, element type and mesh size definition, interaction property definition, loading condition and boundary condition. Firstly, the material property definition was carried out to define all the necessary material properties, including the old and new concrete properties. For the element type and mesh size, the element for concrete specimen had to be decided based on the available element given in ABAQUS software and the optimum mesh size had to be defined considering time efficiency and accuracy of the result. Next is the definition of the interaction properties, this step helps to define the bond condition for concrete to concrete and concrete to steel plate. As for the loading condition, it was only defined according to the specimen specification. Finally, the translational degrees of freedom for the support and loading conditions were defined in the boundary condition definition.

3.4.1 Material Properties

The material properties that required to be defined in this study were only the old concrete and new concrete. Thus, the material properties required to be used for defining the concrete behaviour is density, elasticity and the parameters required in concrete damaged plasticity model.

3.4.1.1 Density, Elasticity and Poisson Ratio

Concrete properties are mostly defined by reference to EN 1992-1-1:2004 (European Commission, 2004). The density of concrete is 2400kg/m^3 (Dorf, 2018). The strength of concrete for both old and new were taken from the specimen suggested by Wu, Ayinde and Zhou (2023) in their study which are 28.0 MPa and 43.0 MPa respectively. The compressive strength of the concrete was then used to find the elasticity for each part, which is 30 GPa for the old

concrete and 34 GPa for the new concrete. The Poisson's ratio for normal concrete is 0.2.

3.4.1.2 CDP Model Parameters

There are several parameters had to input to the CDP model which are dilation angle (ψ), eccentricity (ε), ratio of initial equibiaxial compressive yield stress to initial uniaxial compressive yield stress (f_{b0}/f_{c0}), ratio of the second stress invariant on the tensile meridian to that on the compressive meridian (K_c), viscosity parameter (μ), compressive behaviour and tensile behaviour.

The study by Wu, Ayinde, and Zhou (2023) used the ABAQUS default CDP model parameters: ψ = 38, ε = 0.1, f_{b0}/f_{c0} = 1.16, K_c = 2/3, μ = 0. However, the use of a zero-viscosity parameter can lead to convergence problems in numerical simulations. To address this, Demir et al. (2018) recommend an optimal viscosity parameter of μ = 0.0005. This value has been shown to produce highly accurate numerical results in terms of load-displacement behaviour, closely matching experimental results. Increasing the viscosity parameter beyond this value may lead to results that differ from experimental data. Table 3.4 shows the summary of the CDP model parameters used in this study.

Table 3.4: CDP Model Parameters.

Parameter	Symbol	Value
Dilation angle in degrees	ψ	38
Flow potential eccentricity	ε	0.1
The ratio of the initial equibiaxial compressive yield stress to the initial uniaxial compressive yield stress	f_{b0}/f_{c0}	1.16
Ratio of the second stress invariant on the tensile meridian to that on the compressive meridian (for maximum principal stress)	k_c	0.667
Viscosity parameter	μ	0.0005

Besides that, compressive and tensile behaviour needed to be determined to fully define the CDP model. Firstly, the definition of the concrete behaviour is based on the guidelines given in EC2. The uniaxial stress-strain curve of concrete was used to illustrate the non-linear characteristics of both old and new concretes. In the case of concrete under compression, the values for the plotting of the curve are derived from the concrete compressive strength, f_{cm}. The equation for the stress-strain relationship is given in Equation 3.1, extracted from EC2. Table 3.1 in EC2 was used to determine the elastic stiffness (elasticity) of the concrete, E_{cm}, the plastic strain under compression, ε_{c1}, and the ultimate strain under compression, ε_{cu1} according to the f_{cm} of the concrete used. Then, the constant, η, was obtained using Equation 3.2, while the constant, k, was obtained using Equation 3.3. The value of both constants was then computed based on the f_{cm} of the old and new concretes which are 28 MPa and 43 MPa respectively. Then, the uniaxial stress-strain relationship curve (σ_c against ε_c) by using Equation 3.1 and the result for both concrete grades are shown in Figure 3.7.

$$\frac{\sigma_c}{f_{cm}} = \frac{k\eta - \eta^2}{1 + (k-2)\eta} \tag{3.1}$$

$$\eta = \frac{\varepsilon_c}{\varepsilon_{c1}} \tag{3.2}$$

$$k = 1.05E_{cm} \times \frac{|\varepsilon_{c1}|}{f_{cm}} \tag{3.3}$$

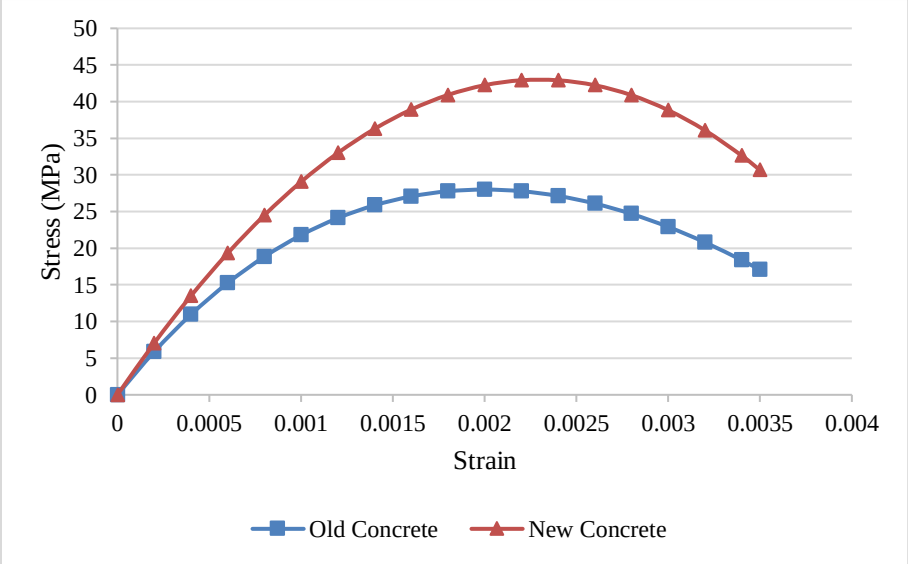

Figure 3.7: Uniaxial Stress-Strain Curves under Compression.

Meanwhile, the definition of the compression behaviour of the CDP model cannot be fully defined by using only the uniaxial compressive stress-strain relationship. The calculation of the relationship between inelastic strains, $\widetilde{\varepsilon_c^{in}}$, and compressive stresses, σ_c, was also carried out as these parameters are the essential parameters to be input into the CDP model. To obtain $\widetilde{\varepsilon_c^{in}}$, Shamass, Zhou, and Alfano (2015) suggested that it is necessary to convert the total strain to the elastic strain, ε_{oc}^{el}, corresponding to the undamaged material using Equations 3.5. The total strain was then subtracted from the ε_{oc}^{el} to obtain the $\widetilde{\varepsilon_c^{in}}$ as shown in Equation 3.4. Figure 3.8 shows the relationship between the compressive stress and the inelastic strain used in the compressive behaviour of the CDP model.

$$\widetilde{\varepsilon_c^{in}} = \varepsilon_c - \varepsilon_{oc}^{el} \tag{3.4}$$

$$\varepsilon_{oc}^{el} = \frac{\sigma_{c0}}{E_{cm}} \tag{3.5}$$

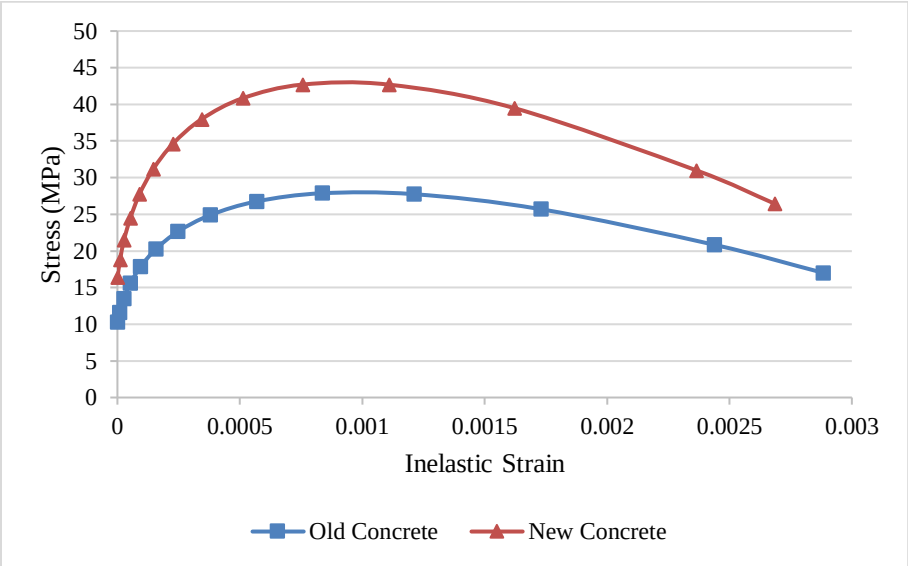

Figure 3.8: Graph of Compressive Stress against Inelastic Strain.

Besides that, the compressive damage parameter, d_c, must be defined for every inelastic strain level. It starts from 0 to 1. The value of d_c is obtained only for the descending slope (after the peak stress) of the of the stress-strain curve of concrete in compression as shown in Figure 3.9. Equation 3.6 was used

to calculate the corresponding damage parameters for each of the compressive stresses experienced by the concrete. Figure 3.10 shows the relationship between the compressive damage parameter and the inelastic strain used in the compression damage of the CDP model.

$$d_c = \begin{cases} 0 \\ \frac{f_{cm}-\sigma_c}{f_{cm}} \end{cases}, \begin{matrix} \varepsilon_c < \varepsilon_{c1} \\ \varepsilon_c \geq \varepsilon_{c1} \end{matrix} \qquad (3.6)$$

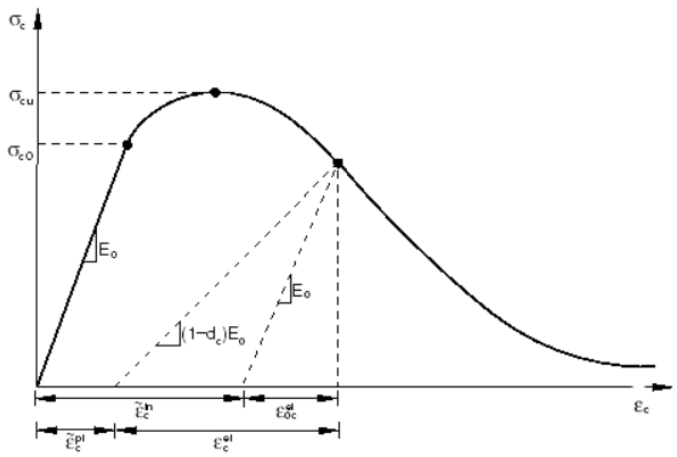

Figure 3.9: Definition of the Compressive Inelastic Strain and Damage Parameters under Uniaxial Compressive Stress-Strain Curve.

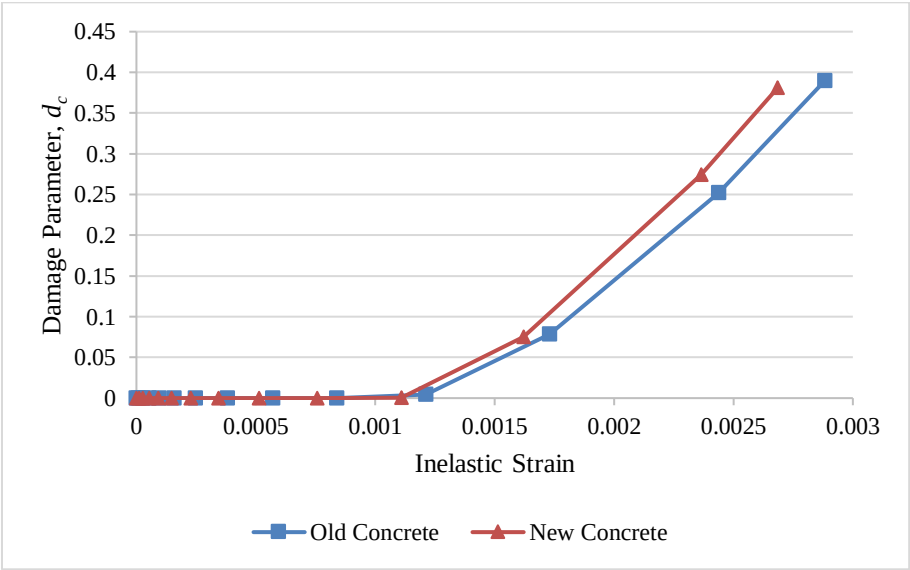

Figure 3.10: Graph of Compressive Damage Parameter against Inelastic Strain.

For tensile behaviour, EC2 stated that the tensile stress in concrete increases linearly with increasing strain until the concrete reaches its cracking strain (ε_{cr}). Beyond this point, the tensile stress is gradually reduced to zero along a tensile stiffening path. Wu, Ayinde, and Zhou (2023) stated that the crack opening, denoted as "w" is measured as it reaches w_1 and w_2, and it is associated with the fracture energy, G_F. Equations 3.9 and 3.10 were used to obtain the values of w_1 and w_2 and Equations 3.7 and 3.8 were used to calculate the tensile stress at a certain displacement. The bilinear stress-displacement curves under tension as shown in Figure 3.11 and the tensile damage parameter-displacement relationship as shown in Figure 3.12 were taken from the reference paper by Wu, Ayinde, and Zhou (2023).

$$\sigma_{ct} = f_{ctm} \cdot (1.0 - 0.82 \frac{w}{w_1}) \tag{3.7}$$

$$\sigma_{ct} = f_{ctm} \cdot (0.25 - 0.05 \frac{w}{w_1}) \tag{3.8}$$

$$w_1 = \frac{G_F}{f_{ctm}} \tag{3.9}$$

$$w_2 = \frac{5G_F}{f_{ctm}} \tag{3.10}$$

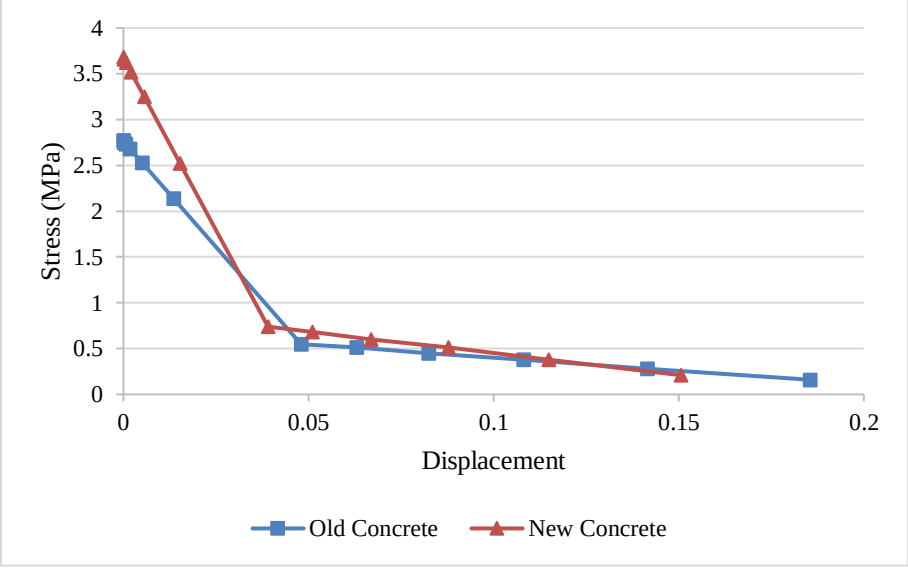

Figure 3.11: Stress-Displacement of Old and New Concrete under Tension.

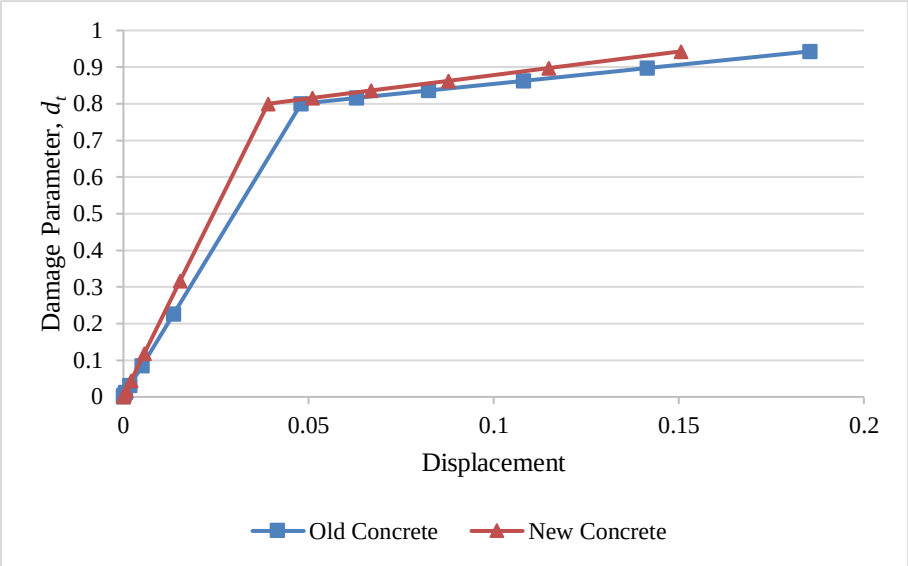

Figure 3.12: Graph of Tensile Damage Parameter against Displacement.

3.4.2 Mesh Element and Mesh Size

The double shear test specimen consists of three parts which are old concrete, new concrete and plate. The old and new concrete parts for the specimen were modelled as C3D8R. The top and bottom plates cannot be meshed as they have been modelled as a 3D analytical rigid shell.

Wu, Ayinde and Zhou (2023) suggested that in order to reduce the analysis time, the mesh distribution should be varied throughout the specimen, which fine meshes should be assigned at the interface region to obtain accurate interface behaviour. The authors suggested that a mesh size of 3 mm at the interface was suitable for the analysis. Therefore, a total mesh size of 15 mm was used in this study and 3 mm mesh seeds were implanted in the interface region. Figure 3.13 shows the meshing of the model to be used in the numerical simulation.

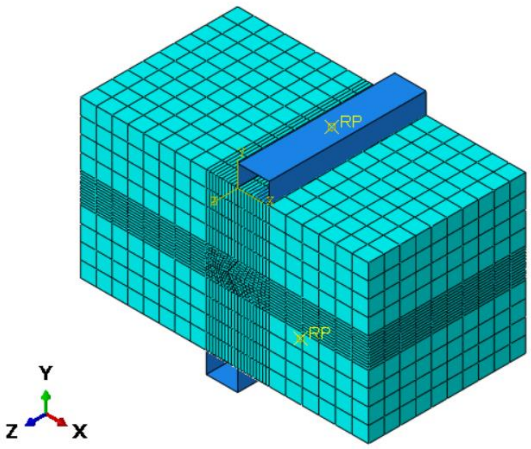

Figure 3.13: Meshing of Model.

3.4.3 Steps, Simulation of Top and Bottom Plate, Loading and Boundary Condition

In this study, two general static steps were defined. The first step was used to apply the confining pressure gradually to prevent the specimen from experiencing a sudden load and causing instability in the concrete mesh node. The second step was then defined to apply the vertical load at the concrete interface to generate the shear load. The load-mechanical pressure was used to define the confining pressure. The horizontal compressive load at the end of the specimen for the specimen consisting of 1.0 MPa confining pressure.

Thanks to the symmetry of the specimens, only half of it was required to be modelled, and an x-symmetry boundary condition was applied at the cut. The reference point of the base plate was constrained against all translational and rotational degrees of freedom to ensure that the shear loading condition was not interrupted by the rotation and translation of the support plate. Meanwhile, the reference point of the loading plate was used to define the displacement-controlling load that applied the shear load to the specimen. The interaction if the interface between the analytical rigid support and the concrete was defined as a “Hard” contact and assigned with a 0.2 friction coefficient. Figure 3.14 shows the boundary condition applied to the specimen model.

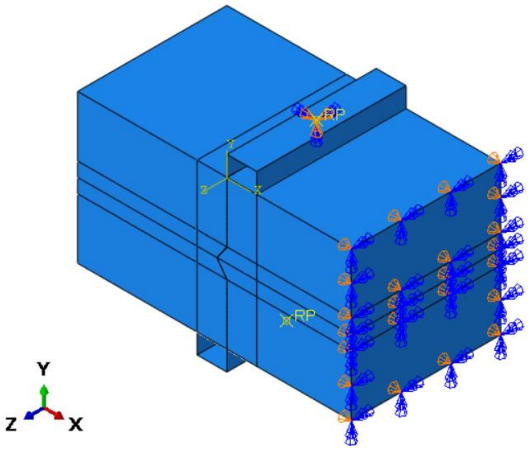

Figure 3.14: Loading and Boundary Condition of Model.

3.4.4 Old-to-New Concrete Interface Model Properties Definition

In this study, the interaction between the old and new concrete interface is similar to the cold joint in the real scenario. Therefore, the interaction property cannot be defined only by the tangential and normal behaviour provided by ABAQUS. By comparing the results obtained by Wu et al. (2023) and Ayinde et al. (2022), it was clearly shown that the most suitable modelling approach to model the concrete interface properties was by using the combination of cohesive behaviour, tangential behaviour and normal behaviour.

The cohesive behaviour used in the ABAQUS software is the application of the traction-separation model. Figure 3.15 shows a typical illustration of the response of the traction-separation model. It can be seen that the response of model follows the elastic trend at the pre-damaged stage, then the damage initiation occurs at the maximum and the damage evolution of the model continues to develop the damage until a complete failure of the traction separation model.

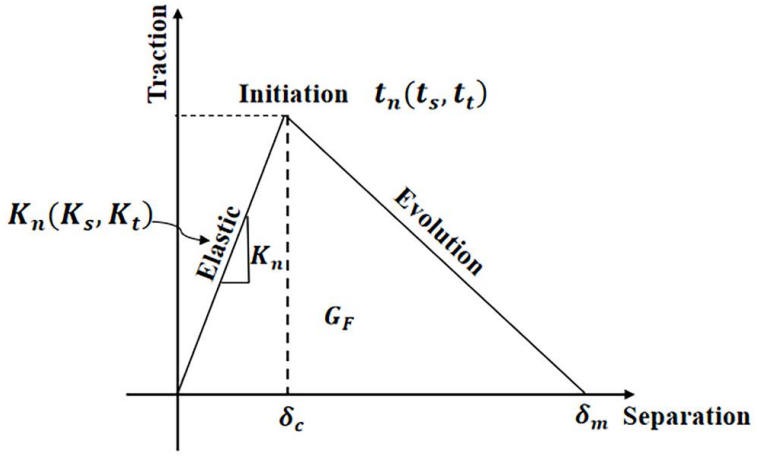

Figure 3.15: Traction-Separation Model.

Zou and Hameed (2018) found that cohesive behaviour was activated once the defined contact experienced shear stress. The authors also found that when the friction and cohesive models were applied simultaneously, frictional behaviour was only activated once cohesive damage was initiated. This means that once the contact experienced the defined maximum shear stress, frictional behaviour was activated to further counteract the excessive shear stress. Thus, there was a transition from pure cohesive behaviour (pre-damaged stage) to a combination of cohesive and frictional behaviour (damage evolution stage) to pure frictional behaviour (complete interface failure stage).

These findings had clearly shown that the combination of cohesive and tangential behaviour could work well to simulate the response of the concrete-to-concrete interface to the shear stress experienced. In order to define the surface-based cohesive interface property, some of the specific parameters were characterised to define the complete interface model. The required parameter was the stiffness (K), the damage initiation (δ_c), and the damage evolution based on total/plastic displacement (δ_m).

Firstly, to determine the value of isotropic uncoupled stiffness components, the equation suggested by Al-Fasih et al. (2021) was used as shown in Equation 3.11.

$$K_s = \frac{S_{max}}{\delta_s^{init}} \tag{3.11}$$

where

K_s = interface stiffness,

S_{max} = interface shear strength at crack initiation,

δ_s^{init} = displacement at crack initiation.

Based on the experimental results obtained by Wu, Ayinde and Zhou (2023), the total crack loads extracted were 77 kN for R01 and 98 kN for R02. The crack loads for both specimens were then substituted into Equation 3.11 and modified to obtain the interface stiffness. As for the damage initiation and damage evolution, the crack displacement of the specimen was extracted to define the maximum separation for the damage initiation criteria, while the displacement at the ultimate load was extracted to define the total/plastic displacement for the damage evolution with linear softening law.

Meanwhile, for normal and tangential behaviour, "Hard" contact was used to define normal behaviour, while the friction model with penalty friction formulation was used to define tangential behaviour. The residual stress was used to determine the friction coefficient, μ (Wu, Ayinde and Zhou, 2023). Therefore, a trial-and-error method was used to find the appropriate value of μ with a benchmark value of 0.56 suggested by Wu, Ayinde and Zhou (2023). Table 3.5 shows the summary of the concrete interface model used in the simulation.

Table 3.5: Concrete-to-Concrete Interface Model Parameter.

Specimen	K	δ_c	δ_m	μ
R01	1.17	0.73	0.73	0.5
R02	1.17	0.73	1.23	0.5

3.5 Result Verification

To assess the reliability and accuracy of the model, a validation process was conducted by comparing the behaviour of numerical simulated reference specimens with experimental data obtained from the study conducted by Wu, Ayinde, and Zhou (2023). The normalised shear stress-slip curve was selected as the benchmark measurement for verification purposes. Additionally, the failure mode observed in the experimental results was also be used to compared

with the DAMAGET contour to validate the numerical model. By employing this empirical result validation approach, it helped in determine whether the numerical model able to accurately predict the behaviour of the reference specimen. If any disparities are identified between the model and real experiment results, correction of the model was done by modifying the concrete-to-concrete interface model parameters.

3.6 Numerical Output Acquisition

This study investigates the behaviour of concrete interfaces with a rectangular roughness tooth. In order to understand this behaviour, three key results were investigated, namely the normalised shear stress-slip relationship, the internal stress distribution and the damage visualisation. Firstly, load-slip relationships were obtained for each specimen and used to calculate the normalised shear stress. The normalised shear stress-slip response of each specimen was then plotted to analyse the effect of tooth thickness on shear capacity under different pressure conditions. Secondly, the maximum principal stress contours were obtained to identify the regions of tension within the concrete. According to Ge and Sinha (2015), this contour was used to identify the internal tension stress within the model. Finally, the DAMAGET contour obtained from the numerical results revealed the location and extent of the tension cracks. By visualising these cracks, the structural integrity of the interface was assessed, and potential failure mechanisms associated with the tooth were identified. The combination of these analyses provided a comprehensive understanding of how the rectangular roughness tooth influences the behaviour and potential failure mechanisms of concrete interfaces under varying pressure conditions.

3.7 Calculation for Normalised Shear Strength

It was necessary to perform the calculation to validate the numerical result against the experimental result because the experimental result used the normalised shear strength to account for the variation of concrete strength at the interface (Wu, Ayinde, and Zhou, 2023). This additional calculation procedure is in accordance with AASHTO and ACI requirements. The normalised shear strength for each data point was obtained from Equation 3.12.

$$\tau = \frac{P}{2A\sqrt{f_c'}} \quad (3.12)$$

where

τ = normalised shear strength (MPa).

P = total shear load distributed over two loading plates (N).

f_c' = cylindrical compressive strength of old concrete ($f_c' = 0.8f_{cu}$) in MPa.

f_{cu} = cubic compressive strength.

3.8 Summary

The methodology of this study was divided into two phases, the planning phase, and the modelling phase. The planning phase consisted of planning the workflow of the study and determining the specification of the specimen. Next, the historical work of Wu, Ayinde and Zhou (2023) was studied, and reference specimens were selected for modelling. Reference and test specimens were then specified by reference to the historical work.

In the modelling phase, ABAQUS software was used to model and simulate the specimen. The modelling process included the definition of concrete properties, boundary conditions, loading conditions, meshing and interaction. Validation and correction of the numerical model was also carried out to ensure the accuracy of the model. This validation process was carried out by comparing the numerical results with the experimental results obtained by Wu, Ayinde and Zhou (2023). When the desired model was obtained and the first objective of this study was achieved, the specimens with different rectangular roughness tooth thickness were modelled and the simulation was carried out.

Once the simulation process was completed, the results of all numerical models such as von Mises stress contours, DAMAGET contour and load-slip relationship were extracted to achieve the second objective. After the numerical results were interpreted by identifying the relationship between the tooth thickness and the shear capacity of the old-to-new concrete interface, and the final study objective is achieved.

CHAPTER 4

RESULTS AND DISCUSSION

4.1 Introduction

This chapter discussed the numerical results obtained by using the ABAQUS software to simulate the behaviour of all the specimens. Specifically, the results of the reference specimens and two batches of test specimens, totalling 20 specimens, were discussed. This discussion included analysis in terms of normalised shear stress-slip curves, maximum principal stress contour (S, Max. Principal), and concrete tensile damage contour (DAMAGET).

This discussion section begins with the discussion of the validation of the results of the reference specimens, R01 and R02, with the experimental results obtained by Wu, Ayinde and Zhou (2023). The comparison was carried out to validate whether the modelling approach and the parameters chosen for the software input data were able to replicate the real behaviour of the specimens. The results were then discussed in three subsequent sections, including an exploration of the influence of varying the thickness of the rectangular roughness tooth under both conditions without and with 1.0 MPa confining pressure on the shear behaviour of the concrete interface. Comparisons were made between nine specimens in each batch in order to evaluate and find the most suitable geometry parameter of the specimen with the highest performance and to make an accurate conclusion. The influence of the confining pressure was also investigated.

4.2 Data Validation of Reference Specimens

To assure the accuracy and reliability of the numerical model, it is important to validate the numerical results. The focus of this section is on validating the results of the reference specimens R01 and R02 by comparing them with the respective experimental data obtained by Wu, Ayinde and Zhou (2023). The comparison process included the analyse of normalised shear slip-slip curves and DAMAGET contours.

4.2.1 Specimen R01

The first reference specimen, R01, was simulated without applying the confined pressure at both ends of the specimen. The normalised shear stress-slip curve and the failure mode were used to validate the numerical model. Figure 4.1 shows the comparison between the experimental and numerical stress-slip curves.

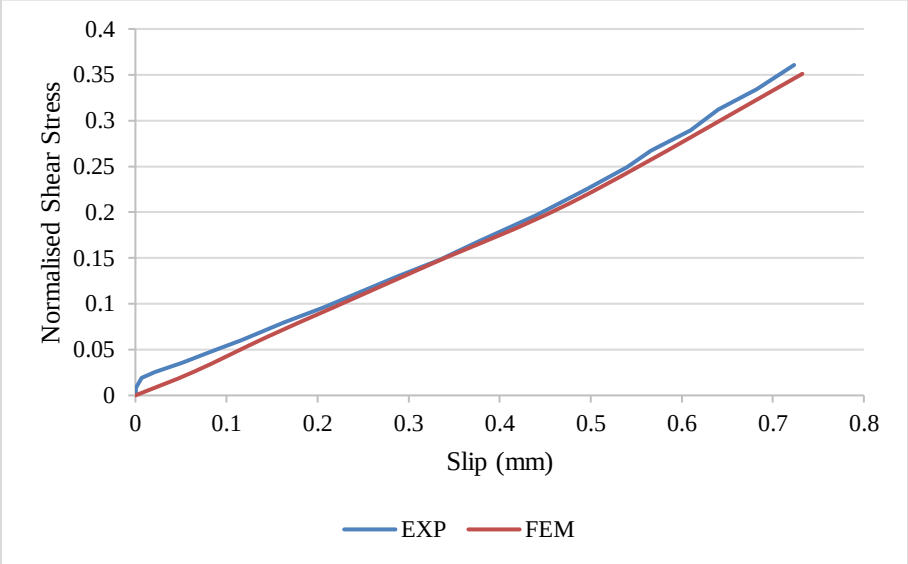

Figure 4.1: Experimental versus Numerical Stress-Slip Curve of R01.

The graph shows an almost linear relationship between normalised shear stress and slip for both the experimental and numerical results, with the model closely following the curve up to the peak shear stress. When interpreting the simulation result in terms of normalised shear capacity, the error between the experimental and numerical method is relatively small (2.5%). The small variation suggests that the constructed numerical model is capable of predicting the desired result following the real behaviour of the specimen.

Figure 4.2 shows the failure mode for the experimental result of R01 obtained by Wu, Ayinde and Zhou (2023). The authors observed adhesive failure occurred at the interface, but no cohesive failure was observed. Only the adhesive failure mode occurred because once the interface separated, there was no normal force to maintain the contact. Therefore, the specimen was unable to sustain the shear load for as long as the interface failure occurred.

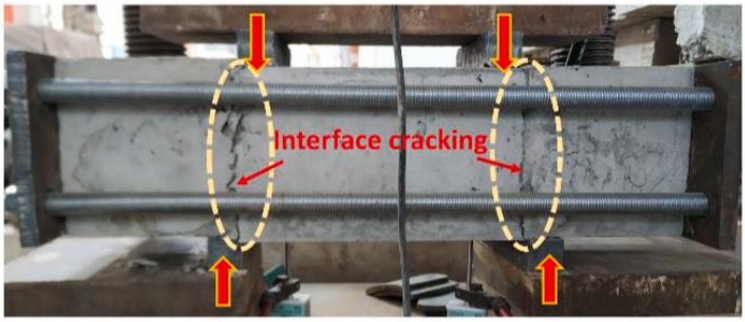

Figure 4.2: Interface Failure (Wu, Ayinde and Zhou, 2023).

Figure 4.3(a) presents the DAMAGET contour obtained from the simulation results at the frame where the specimen failed. There is no observable failure in either the old or new concrete parts which is consistent with the experimental finding of no cohesive failure. However, a detailed evaluation of the interface revealed other finding in the interface region as shown in Figure 4.3(b). An obvious slip can be observed in the interface region, together with an opening at the bottom, which could potentially indicate crack initiation. This finding is similar to the observations made by Wu, Ayinde and Zhou (2023). Unfortunately, due to the limitations of the surface-based cohesive elements used in this study, there is currently no suitable method to detect cracking at the interface. Table 4.1 summarises of the comparison between the experimental and numerical results.

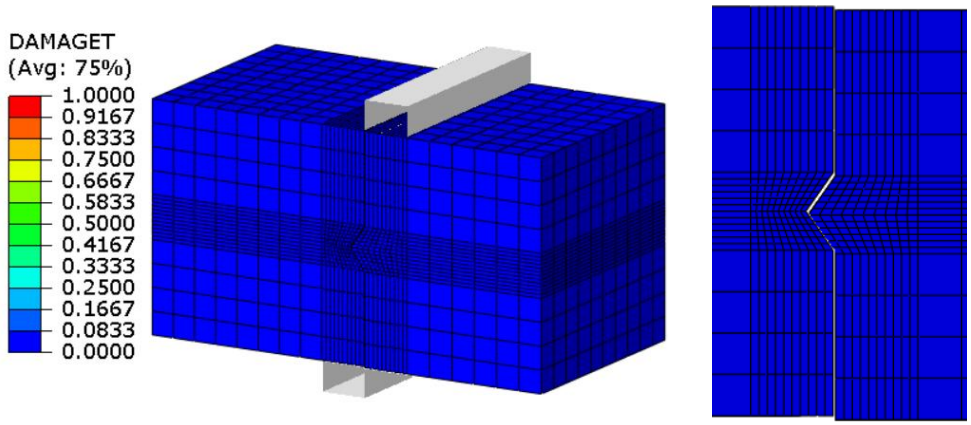

(a) DAMAGET Contour (b) Interface Slip

Figure 4.3: Visualisation of Numerical Result of R01 (a) DAMAGET Contour and (b) Interface Slip.

Table 4.1: Summary of Experimental and Numerical Results of R01.

Method	Normalised Shear Capacity	Percentage Error (%)	Failure Mode
Experimental	0.360	-	Adhesive failure
Numerical	0.351	2.5	Adhesive failure

In overall, a comparison was made between the results of a numerical model and experimental data for a concrete specimen. The comparison shows that the model successfully predicted the shear stress-slip behaviour up to the peak stress with a small error. Both experimental and numerical results showed adhesive failure at the interface, but the model was unable to capture crack initiation due to limitations in the approach used.

4.2.2 Specimen R02

Another reference specimen, R02, was simulated under a load condition of 1.0 MPa confining pressure applied at both ends. To validate the accuracy of the numerical model, a comparison was made between the normalised shear stress-slip curve and the failure mode, similar to validation process in R01. Figure 4.4 shows the comparison for specimen R02, including both the experimental and numerical stress-slip curves.

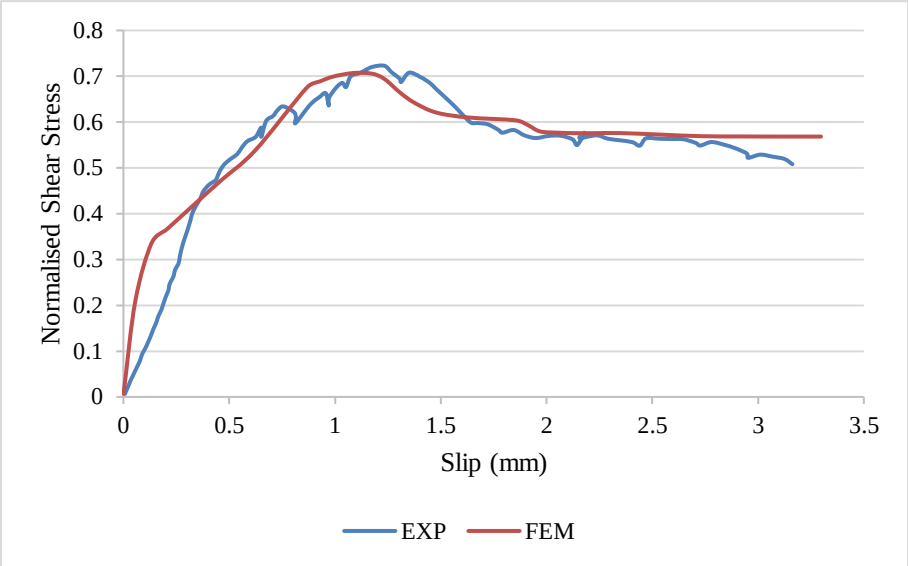

Figure 4.4: Experimental versus Numerical Stress-Slip Curves of R01.

Although the numerical model shows a higher initial stiffness compared to the experimental results, it shows a good agreement with the overall shear behaviour of the specimen. This discrepancy in initial stiffness can be attributed to the perfect state in the simulation. The simulated concrete parts and their interface are likely to be in a perfect and homogeneous state, as opposed to the imperfections present in the actual experiment due to the distribution of the aggregate, especially in the tooth region. The numerically simulated concrete may have a higher stiffness as the Young's modulus of both the old and new concrete parts may be higher than the actual case as the Young's modulus is extracted from EC2.

Despite the difference in initial stiffness, the stress-slip curves from both experiment and numerical methods show a similar trend after an initial slip of 0.35 mm, with failure occurring at around 3.2 mm in the numerical model. The accuracy of the model is further supported by the minimal error of 3.15% observed in the normalised shear capacity. This indicates that the model can effectively capture not only the peak shear capacity of specimen R02, but also the overall trend of its stress-slip relationship.

Figure 4.5 shows the failure mode observed by Wu, Ayinde and Zhou (2023) for the experimental results of R02. In contrast to R01, which showed only adhesive failure, R02 showed a combination of adhesive and cohesive failure modes. This difference can be attributed to the presence of confining

pressure in R02. The confining pressure allows the specimen to maintain contact between the old and new concrete parts. Consequently, the roughness tooth in R02 is able to resist a greater shear load compared to R01, leading to the observed shear crack of the roughness tooth.

Figure 4.5: Experimental Failure of R02 (Wu, Ayinde and Zhou, 2023).

The numerical model successfully replicated the failure mode and location observed in the experiment. Figure 4.6 shows the DAMAGET contour on the frame corresponding to the experimental failure slip (3.2 mm). Similar to the experimental results, the simulation predicts failure at the root of the roughness tooth, indicating a shear crack at the tooth. This agreement provides a strong validation of the model, suggesting that it can be a reliable tool for simulating a similar outcome to the experimental result. The comparison of the experimental and numerical results is tabulated in Table 4.2.

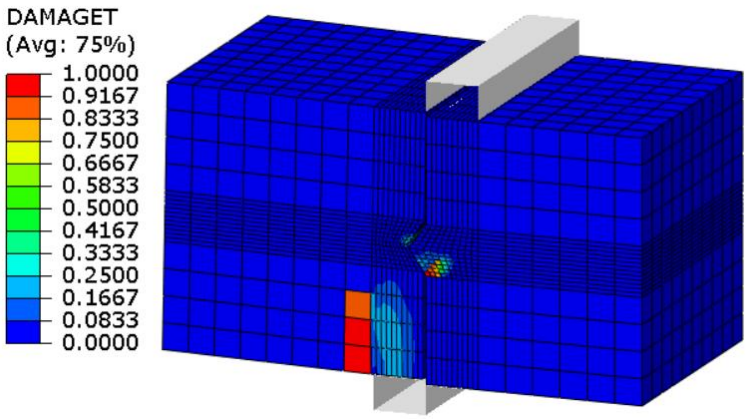

Figure 4.6: DAMAGET Contour of R02.

Table 4.2: Summary of Experimental and Numerical Results of R02.

Method	Normalised Shear Capacity	Percentage Error (%)	Failure Mode
Experimental	0.730	-	Adhesive & cohesive failure
Numerical	0.707	3.15	Adhesive & cohesive failure

In short, the comparison between the result of numerical model with experimental data for a concrete specimen under confining pressure had been done. Despite a higher initial stiffness in the model due to the assumption of perfect materials condition, the overall stress-slip behaviour agreed well with the experiment. The model also successfully captured the combined adhesive and cohesive failure mode observed in the experiment, including the location of the crack, confirming its accuracy for such scenarios.

4.3 Test Specimens without Confining Pressure (Batch A)

This section discusses the Batch A consist of nine specimens (T0-30, T0-35, T0-40, T0-45, T0-50, T0-55, T0-60, T0-65, T0-70) without the confining pressure at both ends of the specimens. These specimens have a rectangular roughness tooth with varying thicknesses from 30 mm to 70 mm, increasing by 5 mm for each specimen. Although the depth of the roughness tooth of all test specimens (10 mm) is the same as the reference specimens, this is to avoid blind speculation to ensure the accuracy of the result. Several numerical results were discussed including normalised shear stress-slip curves, maximum principal stress contours, and DAMAGET contour.

4.3.1 Normalised Shear Stress-Slip Curves

The comparison of the normalised shear stress-slip curve shown in Figure 4.7 shows some clear differences between the behaviour of the tested specimens in Batch A and the reference specimen (R01). The two differences between the results including the residual strength and the stiffness.

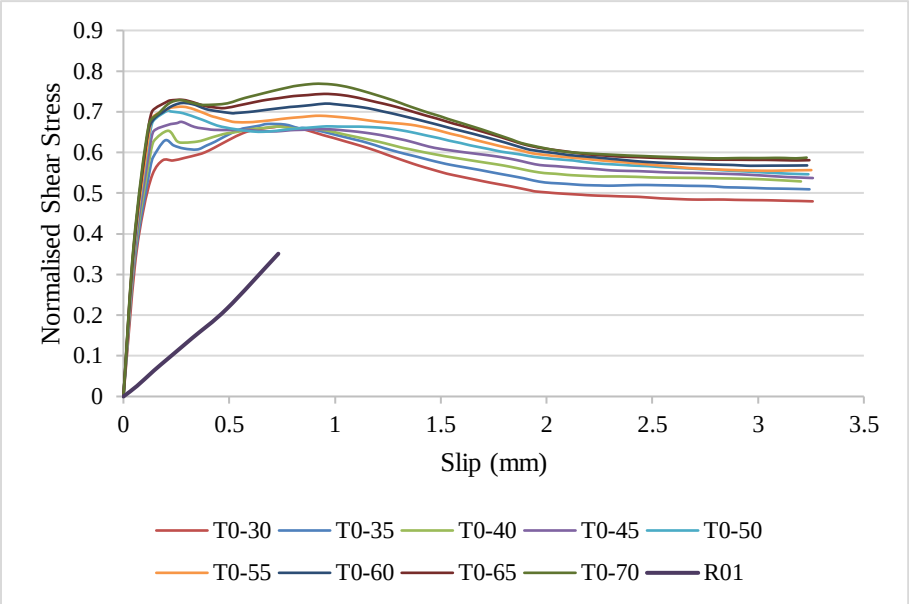

Figure 4.7: Normalised Shear Stress-Slip Curves of Batch A Specimens and R01.

Firstly, the difference in terms of residual strength is due to the different geometries of their roughness tooth. The specimens in Batch A use rectangular roughness tooth that act as hinges. Even after the initial bonding between the interfaces fails, the tooth remains engaged and provide resistance up to a slip of 3.2 mm. This suggests a mechanical locking mechanism provided by the rectangular tooth, which persists even with adhesive failure. Conversely, the reference specimen (R01) uses triangular tooth. The initial resistance is based on interfacial bonding and once this bond is failed, the tooth cannot effectively resist the shear load as there is no external pressure to maintain contact between the interfaces.

Furthermore, the significant difference in initial stiffness observed between the specimens can also be attributed to the different roughness tooth geometries. As the loading mechanism in the Batch A specimens appears to transition to a hinge-like behaviour, the initial interface bond strength may play a less dominant role in directly influencing the overall shear strength. Instead, the strength of the new concrete part (male joint) may become a more dominant factor influencing the interface shear strength. This observation suggests that further investigation of the micro-level load transfer mechanism is required to

definitively determine the influence of interface bonding on the shear strength of the concrete interface with rectangular roughness tooth.

In addition to the influence of different tooth geometry, it is also worth noting how the rectangular tooth thickness affects the normalised shear capacity. Figure 4.8 shows the correlation between normalised shear capacity and maximum normalised shear stress for all Batch A specimens. Linear regression analysis was performed on the data points from 30 mm to 70 mm as shown in Equation 4.1.

$$\tau_t = 0.0026t + 0.5708 \quad (4.1)$$

This equation represents the correlation between normalised shear capacity and tooth thickness. The coefficient of determination (R^2) of 0.9206 indicates that the tooth thickness significantly affects the normalised shear capacity. Moreover, the study shows that a gradual increase in tooth thickness from 30 mm to 70 mm results in a 15.81% increase in normalised shear capacity. This finding underscores the practical significance of tooth thickness in providing a higher normalised shear capacity.

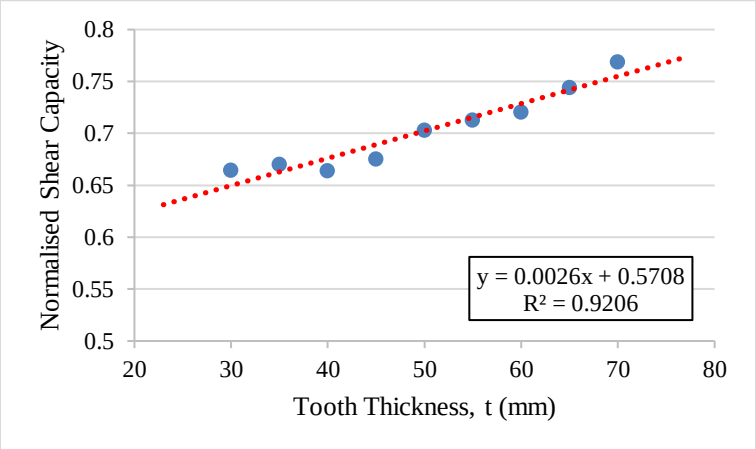

Figure 4.8: Correlation between Normalised Shear Capacity and Tooth Thickness.

Besides that, the analysis of the overall trend of the stress-slip curves for all specimens revealed interesting behaviour in the peak stress region as shown in Figure 4.9. Each specimen consistently exhibited two distinct peak

points, one primary and one secondary. These points are tabulated and plotted in Figure 4.10 and show a trend shift across the specimens. Specimens T0-30 to T0-40 showed a higher primary climax compared to the secondary climax. This trend was reversed for samples T0-45 to T0-55 where the primary peak became lower than the secondary peak. Interestingly, sample T0-60 showed an almost equal value for both peaks, suggesting a potential turning point in this behaviour. Finally, samples T0-65 and T0-70 returned to the original trend with a higher primary peak.

This analysis suggests that the specimens have different abilities to generate shear strength. Specimens T0-30 to T0-40, T0-65 and T0-70 maintained a higher shear strength at the secondary peak. However, specimens T0-45 to T0-55 lacked this ability and the shear strength decreased after the primary climax. The almost equal peaks in T0-60 suggest a possible equilibrium state in this behaviour. While these observations are intriguing, the underlying mechanism remains unclear. Further investigation is required to validate these findings and to determine the reason for the shift in peak behaviour between specimens.

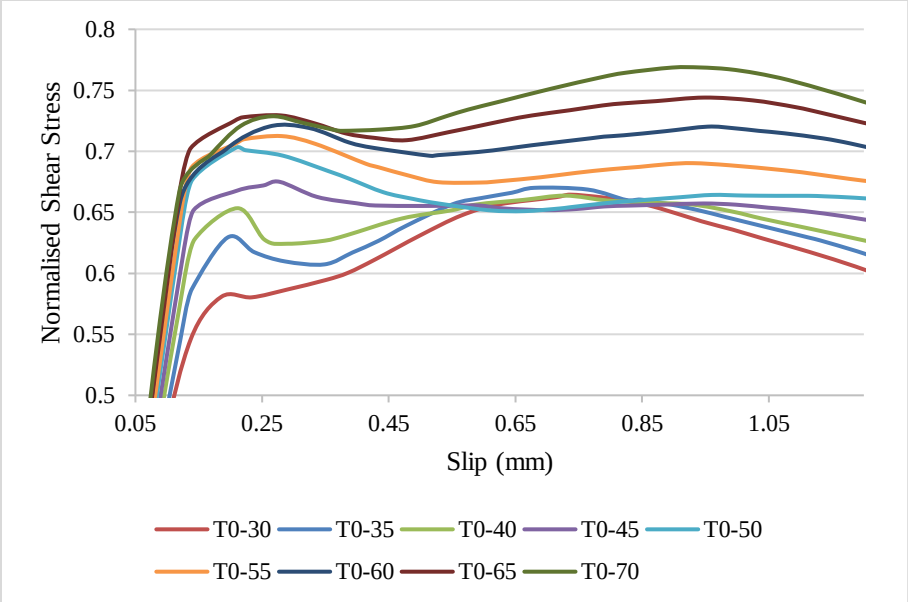

Figure 4.9: Enlarged Stress-Slip Curves of Batch A Specimens at Peak Stress Region.

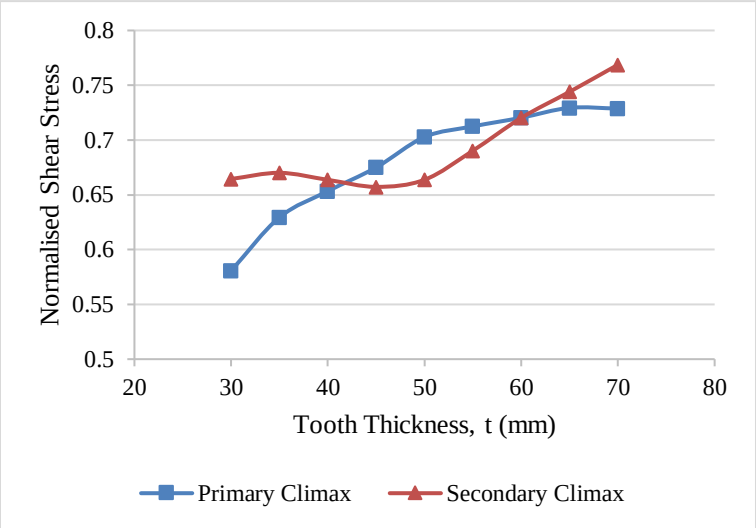

Figure 4.10: Comparison of Primary and Secondary Climax Normalised Shear Stress against Tooth Thickness.

4.3.2 Maximum Principal Stress Contour

Maximum principal stress contours were used to analyse the internal tensile stress distribution in the specimens. Figure 4.11 shows a visualisation obtained from the simulation results at the frame corresponding to the maximum normalised shear stress for the Batch A specimens. To improve the visualisation of the internal tensile stress at the centre of the specimen, a section perpendicular to the z-axis has been applied. For consistent comparison, a common legend was used and restricted to positive stresses representing tensile stress.

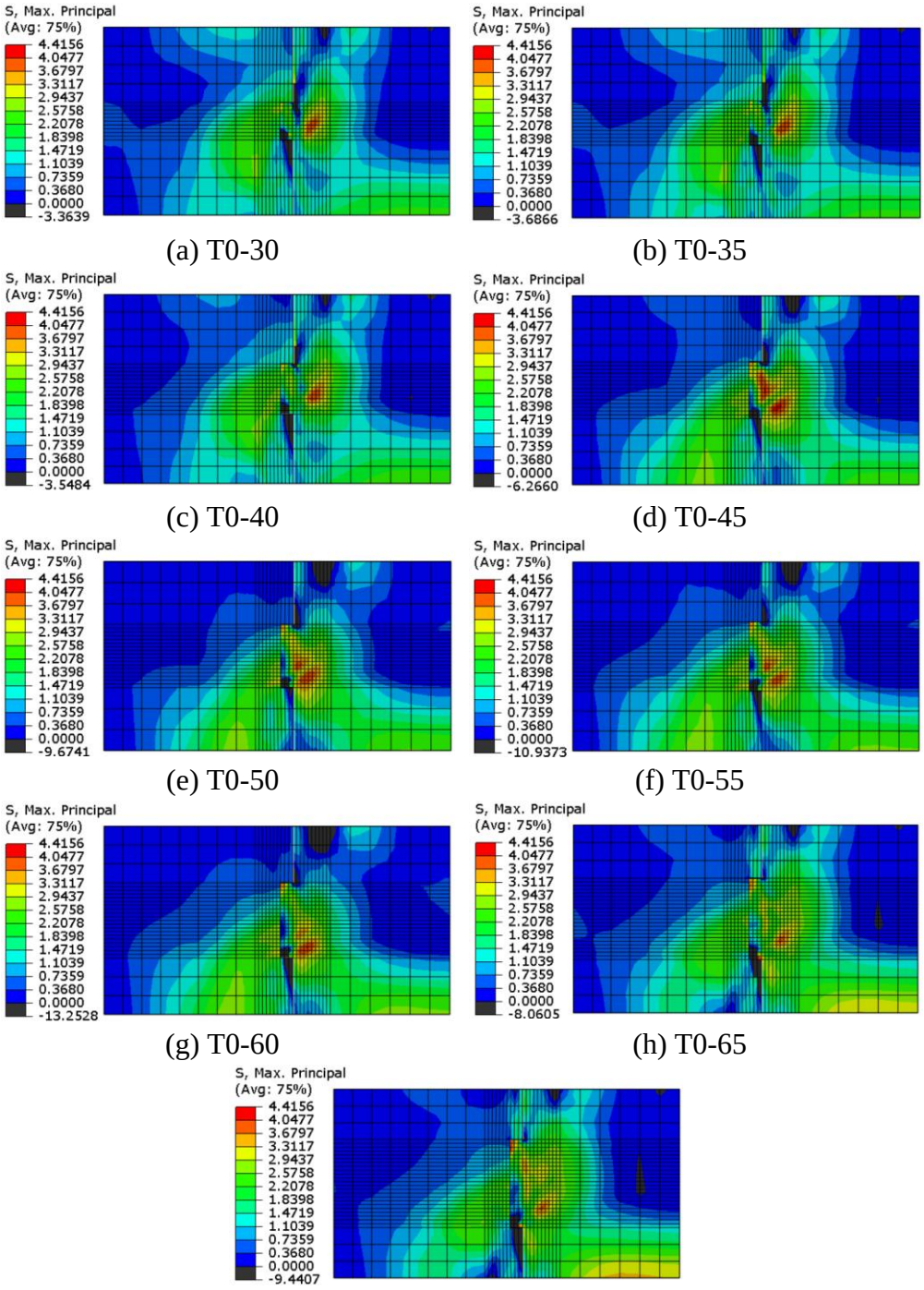

Figure 4.11: Maximum Principal Stress Contours for Batch A Specimens (a) T0-30, (b) T0-35, (c) T0-40, (d) T0-45, (e) T0-50, (f) T0-55, (g) T0-60, (h) T0-65 and (i) T0-70.

Comparison of the contours for each specimen showed that the tensile stress was concentrated at the interface, with similar patterns across all specimens. Interestingly, there was a compressive zone at the top of the tooth in the new concrete part of specimen T0-30. However, this zone gradually

disappeared with increasing tooth thickness and disappeared completely in specimen T0-70. In contrast, the compression zone at the root of the roughness tooth on old concrete parts remained present in all specimens in Batch A.

Finally, the location of the maximum tensile stress was consistently within the new concrete section and close to the roughness tooth. For specimens T0-30, T0-35 and T0-40, it appeared as a single concentrated zone. However, for specimens T0-45 onwards, this zone split into two separate regions. With increasing tooth thickness (T0-70) this fragmentation of the high stress zone became more pronounced. This suggests that the tensile stress contour was influenced by the thickness of the roughness tooth.

4.3.3 DAMAGET Contour

The DAMAGET contour was used as a visualisation approach to indicate the tensile failure that occurred within the specimen model. Figure 4.12 shows the DAMAGET contour extracted at a slip of 3.2 mm, following the failure slip recorded in the reference specimen. Analysis of the contour shows that the contours of all Batch A specimens exhibited cohesive failure, in contrast to the triangular tooth reference specimen (R01) which exhibited no cohesive failure, only adhesive failure. While the cohesive failures were clearly present in the Batch A specimens, the large interface opening at the bottom suggested potential cohesive failure. Therefore, the failure mode of all specimens is a combination of cohesive and adhesive failure.

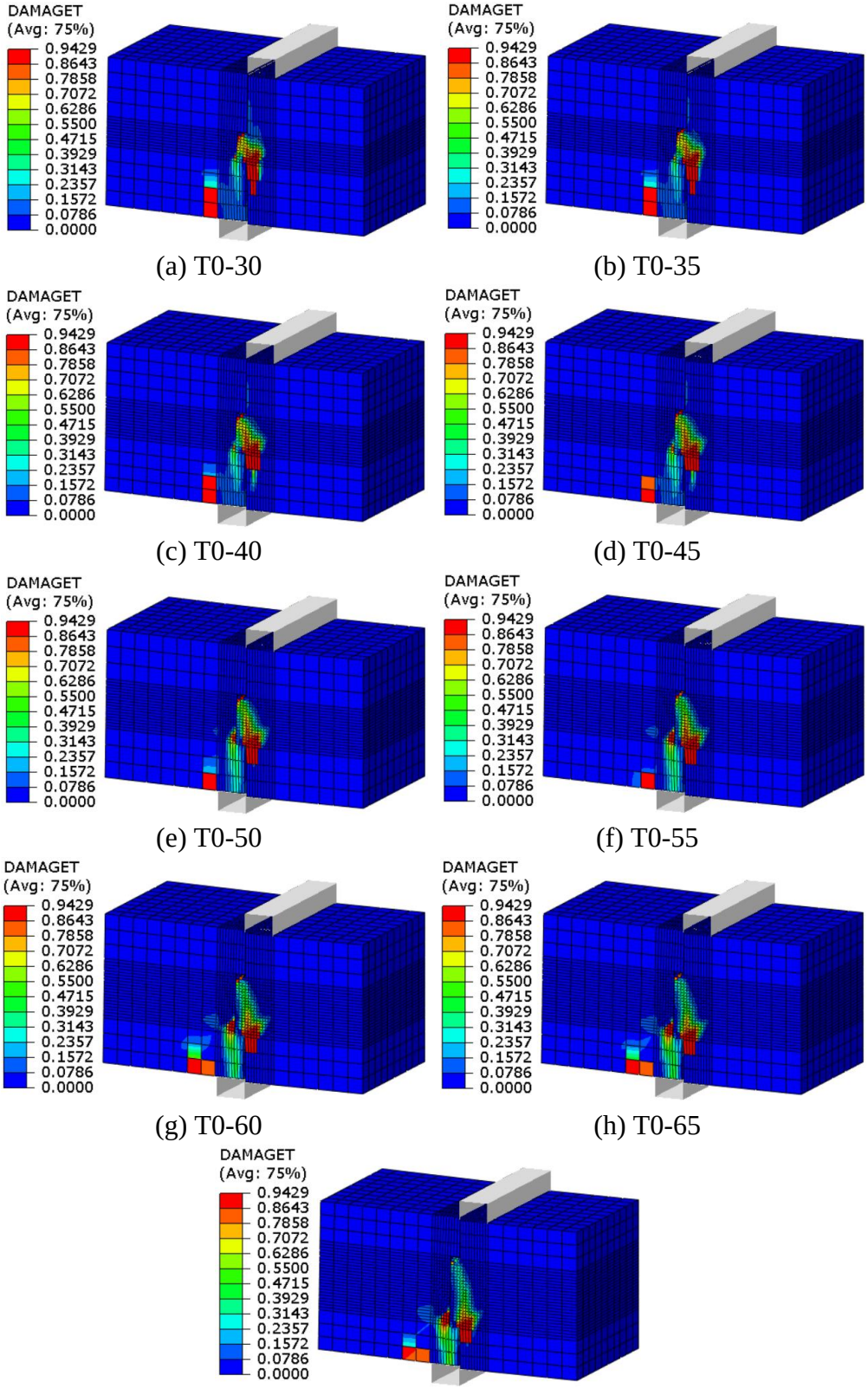

(a) T0-30 (b) T0-35

(c) T0-40 (d) T0-45

(e) T0-50 (f) T0-55

(g) T0-60 (h) T0-65

(i) T0-70

Figure 4.12: DAMAGET Contour of Batch A Specimens (a) T0-30, (b) T0-35, (c) T0-40, (d) T0-45, (e) T0-50, (f) T0-55, (g) T0-60, (h) T0-65 and (i) T0-70.

Besides that, further analysis of these contours revealed a consistent pattern of tensile failure at the base of the roughness tooth in the new concrete part for each specimen. This failure, propagating from the inner corner in all directions, indicated shear failure at this location due to the shear load. This pattern is consistent with the ideal scenario observed in the shear tests by Niwa et al. (2016) and Shamass, Zhou, and Alfano (2015).

Furthermore, a comparison of the DAMAGET contours with the maximum principal stress contours confirmed the following findings. The outer root of the roughness tooth did not fail in tension while the crack progressed from the inner root to the central region below the load plate where the highest tensile stress zone was located. This reinforces the successful transfer of shear load to the roughness tooth and not just through the interface, resulting in a greater shear capacity as previously discussed in the normalised shear stress-slip curve, and also suggests that the shear load transfer mechanism of the rectangular roughness tooth is different from that of the triangular roughness tooth.

4.4 Test Specimens with 1.0 MPa Confining Pressure (Batch B)

Nine specimens (T1-30 to T1-70) in Batch B, which have exactly the same specifications as Batch A with one key difference: the application of 1.0 MPa confining pressure at both ends. The purpose of this investigation is to understand how the confining pressure affects the effectiveness of the rectangular roughness tooth in resisting shear loading. Research by Wu, Ayinde and Zhou (2023) suggests that confining pressure can maintain contact between concrete sections even after interface bond failure. The analysis of Batch B helps to determine whether this pressure improves the performance of the roughness tooth under shear loading. To achieve this, several numerical results were examined, including normalised shear stress-slip curves, maximum principal stress contours and DAMAGET contours.

4.4.1 Normalised Shear Stress-Slip Curve

Figure 4.13 shows the normalised shear stress-slip curves for all nine Batch B specimens alongside the reference specimen, R02. Analysis of the curves comparison reveals two key findings regarding the shear resistance of Batch B

specimens compared to the reference specimen (R02) with a triangular roughness tooth.

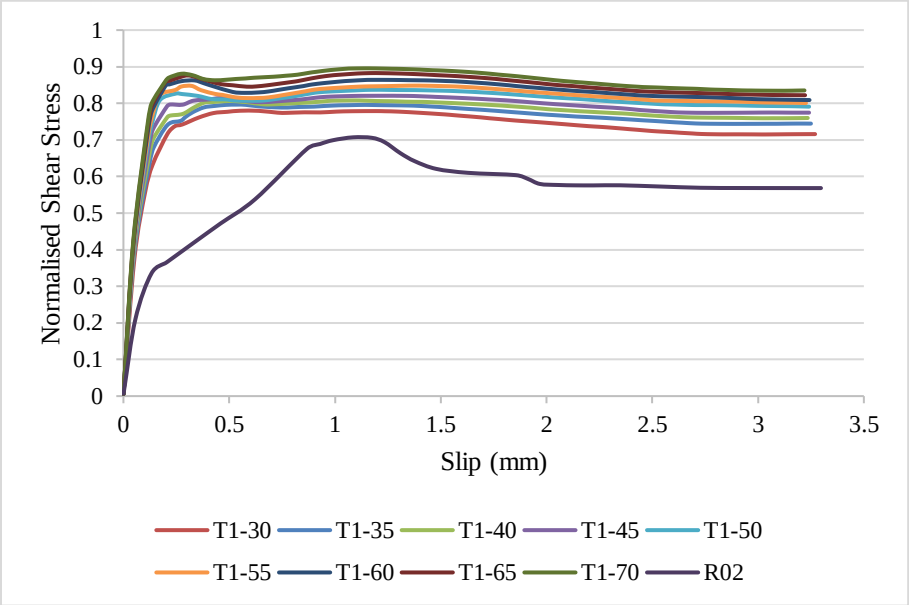

Figure 4.13: Normalised Shear Stress-Slip Curves of Test Specimens in Batch B and R02.

Firstly, the Batch B specimens poses higher post-peak performance compared to R02. All specimens show an initial increase in shear stress as slip increases, indicating elastic behaviour. This is followed by an inelastic state and the peak stress point is reached. Importantly, even after peak stress, Batch B specimens maintain a normalised shear strength between 0.7 and 0.9, indicating good residual strength. In contrast, the reference specimen (R02) achieves a lower peak strength (0.707) and experiences a significant drop (18.53%) in its residual strength. This highlights the advantage of the rectangular roughness tooth in providing a superior ability to resist shear loading after peak stress is reached.

Secondly, the relationship between tooth thickness on shear resistance has been defined to determine the dependency of shear resistance on the tooth thickness. As the graph shows variations in peak shear stress between Batch B specimens, Figure 4.14 examines the relationship between normalised shear capacity and tooth thickness. Linear regression analysis shows a strong correlation (R^2 = 0.9976) between these two variables. This indicates that under

the applied confining pressure of 1.0 MPa, the normalised shear strength of specimens with rectangular roughness tooth is highly dependent on the thickness of the tooth. The result also shows that a gradual increase in tooth thickness from 30 mm to 70 mm results in a 14.87% increase in normalised shear capacity.

In short, Batch B specimens with rectangular roughness tooth exhibit both improved post-peak performance compared to the reference specimen and a dependence of shear strength on tooth thickness.

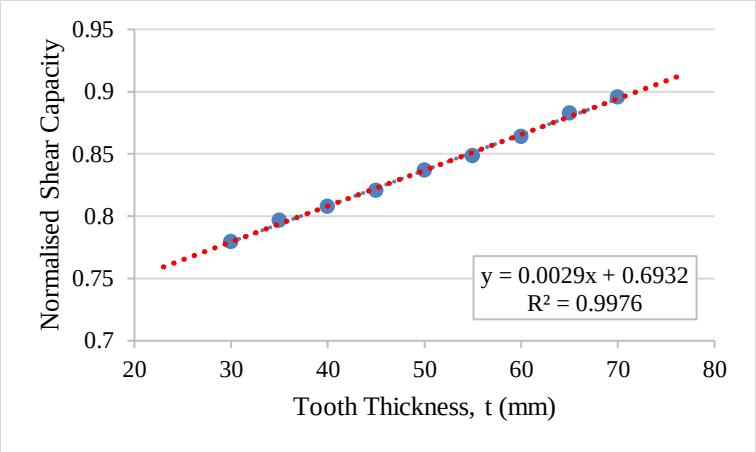

Figure 4.14: Correlation between Normalised Shear Capacity and Tooth Thickness.

4.4.2 Maximum Principal Stress Contours

Figure 4.15 shows the maximum principal stress contours of each Batch B specimen at the frame corresponding to the peak normalised shear strength and a sectional view has been applied in the centre. Analysis of the stress distribution for the Batch B specimens at peak shear strength shows that the tensile stress is concentrated at the interface.

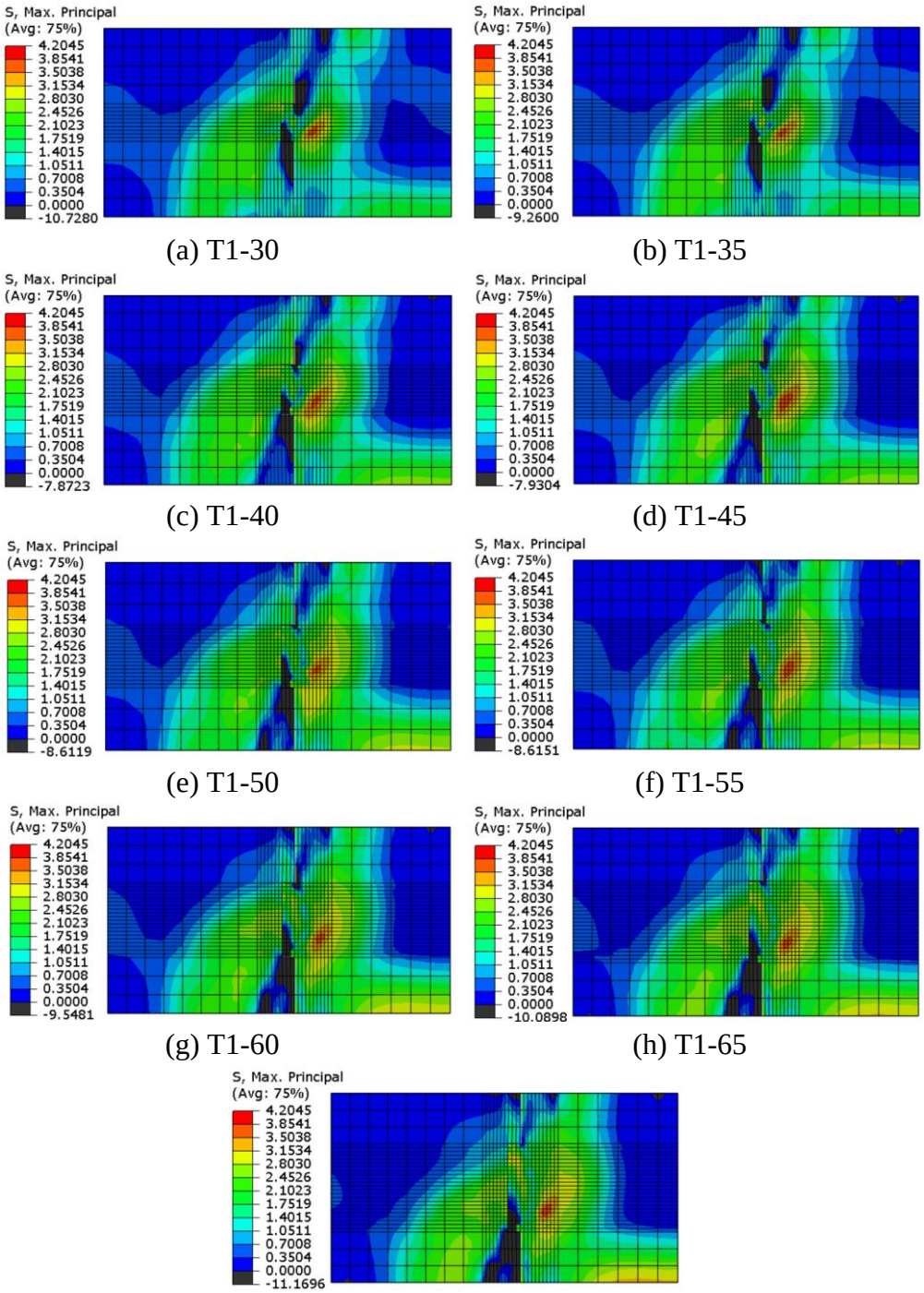

(a) T1-30 (b) T1-35

(c) T1-40 (d) T1-45

(e) T1-50 (f) T1-55

(g) T1-60 (h) T1-65

(i) T1-70

Figure 4.15: Maximum Principal Stress Contours for Batch B Specimens (a) T1-30, (b) T1-35, (c) T1-40, (d) T1-45, (e) T1-50, (f) T1-55, (g) T1-60, (h) T1-65 and (i) T1-70.

Furthermore, for specimens T1-30 and T1-35, a small region of compressive stress can be seen at the bottom edge of the roughness tooth in the old concrete part, and at the top inner corner within the new concrete part.

However, when the tooth thickness increases, the top compressive zone progressively transforms into a tensile zone and disappears completely in specimen T1-70. This result implies that the internal tensile stress is growing beneath the top loading plate as the tooth thickness increases. Moreover, the shape of the compression zone beneath the roughness tooth transforms to a triangular shape starting from T1-40 onwards.

Finally, another significant discovery is that the maximum tensile stress is consistently located within the new concrete part regardless of how the tooth thickness varies. This critical tensile stress is consistently observed diagonally to the root of the roughness tooth, indicating a high likelihood of shear crack initiation at the root of roughness tooth and propagation towards this critical region. The subsequent section will dive into the pattern of the shear crack to provide additional validation of the analysis of this internal tensile stress distribution.

4.4.3 DAMAGET Contour

Figure 4.16 shows the damage (DAMAGET contour) within the Batch B specimens at the failure slip. The contour clearly shows tensile cracks formed at the root of the roughness tooth, confirming the shear failure mode observed by Shamass et al. (2015) and Zhou et al. (2005). Furthermore, increasing the thickness of the roughness tooth resulted in a larger crack area, but the cracks remained in the interface zone. This suggests that the failure location itself is not significantly affected by tooth thickness. However, the total crack area does scale with tooth area.

Moreover, all specimens exhibited an opening at the lower interface below the roughness tooth, indicating adhesive failure (interface bond failure). This adhesive failure, combined with the cohesive failure (shear cracking) observed at the root, suggests a combined failure mode similar to the reference triangular roughness tooth under confining pressure. Aside from that, the presence of microcracking at the base of the old concrete further supports the maximum principal stress analysis.

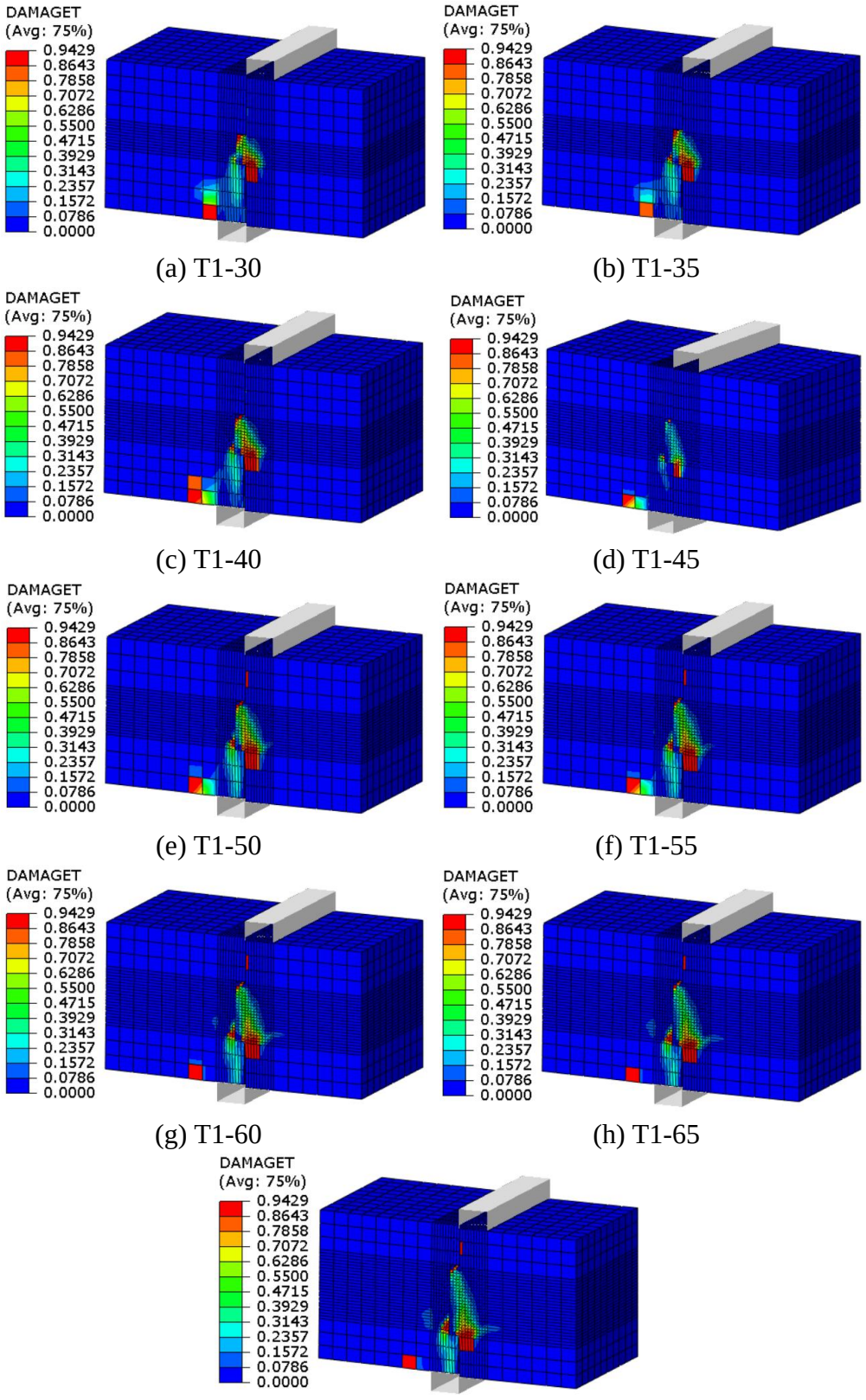

(a) T1-30 (b) T1-35

(c) T1-40 (d) T1-45

(e) T1-50 (f) T1-55

(g) T1-60 (h) T1-65

(i) T1-70

Figure 4.16: DAMAGET Contour of Batch B Specimens (a) T1-30, (b) T1-35, (c) T1-40, (d) T1-45, (e) T1-50, (f) T1-55, (g) T1-60, (h) T1-65 and (i) T1-70.

4.5 Effect of Confining Pressure

According to the findings of Wu, Ayinde and Zhou (2023), the authors found that confining pressure significantly increased the normalised shear capacity compared to specimens without confining pressure. At 1.0 MPa, there is a 102.8% increment in normalised shear capacity. However, the rectangular tooth showed a smaller increase in normalised shear capacity (16.5% to 21.7%) compared to the triangular tooth under confining pressure. This suggests that confining pressure has a less pronounced effect on rectangular tooth specimens.

Meanwhile, it is also important to note that the confining pressure still demonstrably improved the normalised shear capacity of all specimens regardless of tooth thickness. A more detailed comparison of the effectiveness of confining pressure and the visual differences in shear capacity based on tooth thickness is shown in Table 4.3 and Figure 4.17 respectively. Besides, the increase of tooth thickness from 30 mm to 70 mm under Batch A has resulted in a 15.81% increase in normalised shear strength and under Batch B has resulted in a 14.87% increase in normalised shear strength. This finding shows that the presence of confining pressure does not affect the degree of influence of tooth thickness on the shear strength.

Table 4.3: Summary of All Test Specimens.

Tooth Thickness	**Normalised Shear Capacity**		**Percentage of Difference (%)**
	Batch A (T0)	**Batch B (T1)**	
30	0.664	0.780	17.5
35	0.670	0.796	18.8
40	0.664	0.808	21.7
45	0.675	0.821	21.6
50	0.703	0.837	19.1
55	0.712	0.848	19.1
60	0.720	0.864	20.0
65	0.744	0.883	18.7
70	0.769	0.896	16.5

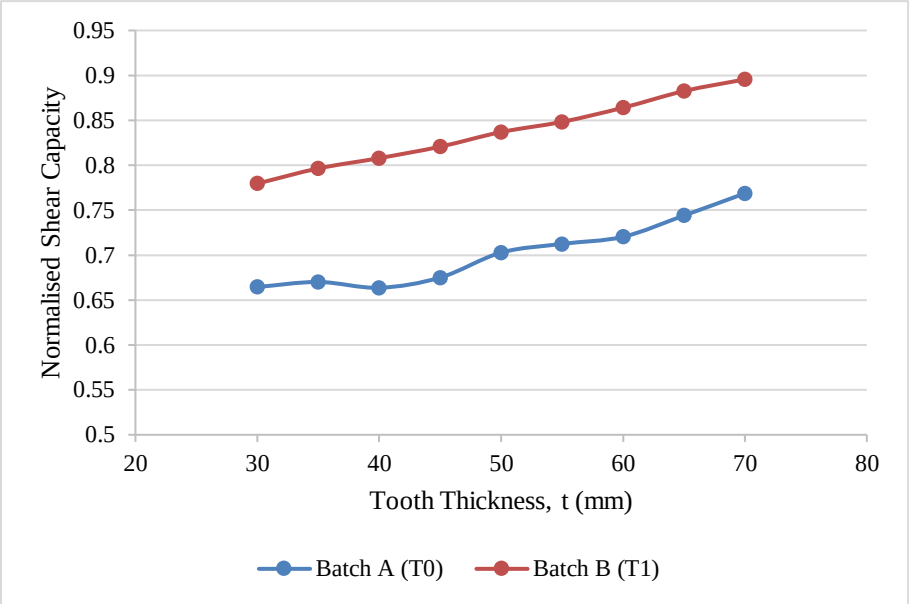

Figure 4.17: Relationship between the Normalised Shear Capacity and Roughness Tooth Thickness for Batch A and Batch B Specimens.

4.6 Summary

In short, the increase in tooth thickness results in a higher normalised shear capacity both with and without confining pressure. The result of both specimens with and without confining pressure shows a strong correlation between tooth thickness and normalised shear capacity. Besides that, the finding reveals that the increase in tooth thickness has a positive effect on shear strength. On the other aspect, the stress-strain curves for the specimens without confining pressure showed a shift in the peak point, indicating the different behaviour to generate residual shear strength. For the specimens with confining pressure, the residual shear strength is more stable compared to the specimens without confining pressure. Furthermore, the tensile stress was consistently located within the new concrete part where within the roughness tooth area, highlighting the importance of the tooth in this shear load transfer regardless of the presence of confining pressure.

The failure mode of all specimens is the same, which is a combination of adhesive and cohesive failure. This means that the shear load is successfully transferred from the top loading plate and through the roughness tooth to the bottom support plate. The shear crack also occurred at the roughness tooth in all specimens indicating cohesive failure. In addition, the shear crack of the

roughness tooth always started from the root and propagated diagonally and is related to the result of the study in Section 2.3.1.

CHAPTER 5

CONCLUSIONS AND RECOMMENDATIONS

5.1 Conclusions

This study has been conducted successfully on the impact of a single rectangular roughness tooth on the shear behaviour of old-to-new concrete interfaces using ABAQUS software. Two types of specimens were utilised to achieve the first objective. The first type included two reference specimens that used for model calibration. Through the comparison of numerical outcomes with existing experimental data, the models attained a high level of accuracy, with errors in the ultimate strength estimates for specimens R01 and R02 remaining below 3.2%. Furthermore, the trends observed in the shear stress-slip relationship from the numerical model closely follow the actual experimental data. The consistency between these results and the failure modes observed in both the numerical and experimental data validated the chosen modelling approach and parameter settings. The model calibrated successfully with the interface parameters, and it was used for further investigation of the following 18 test specimens.

The secondary objective of the study is to identify the failure mode, crack pattern, and normalised shear strength. The reference specimens exhibited various failure modes, with R01 exhibited adhesive failure only while R02 showed a combination of adhesive and cohesive failure. In contrast, all test specimens demonstrated a consistent failure mode characterised by a combination of adhesive and cohesive failure. The crack patterns vary among the reference specimens, with R01 showed interfacial cracking only and R02 showed both interfacial and shear cracking initiated from the root of the roughness tooth and propagating diagonally. However, a consistent cracking pattern emerged for the specimens which is similar to the crack pattern exhibited by R02. Additionally, the normalised shear strength, which was determined using the maximum shear stress experienced by each specimen, was obtained.

The third objective of this research is to examine how the thickness of a tooth affects the shear behaviour of the concrete interface under different

levels of confining pressure. The findings indicate that regardless of changes in tooth thickness or the application of confining pressure, both the failure mode and crack propagation remained consistent. However, there is a notable impact of tooth thickness on shear capacity. In all cases, an increase in tooth thickness corresponded to an increase in shear capacity, regardless of whether confining pressure was present or not. Strong correlation coefficients were obtained for both Batch A (0.9206) and Batch B (0.9976) to further support that their shear capacity is depending on tooth thickness. Additionally, the application of confining pressure had positively influenced shear capacity, resulting in an average increase of 19.2%, while the existence of confining pressure has no significant effect on the degree of influence of tooth thickness on shear strength.

All of the objectives outlined in this study have been successfully accomplished, including the investigation of the effectiveness of a single rectangular roughness tooth on the shear behaviour of the interface between old and new concrete.

In summary, this numerical investigation explored the shear behaviour of concrete interface with a rectangular roughness tooth. Through the development of a reliable numerical model, analysis of failure modes and crack patterns, and identification of the relationship between tooth thickness and shear behaviour, the results demonstrate that tooth thickness significantly impacts shear capacity, with thicker tooth leading to higher shear capacity. Furthermore, the application of confining pressure also has a positive influence on shear capacity but does not improve the effectiveness of roughness tooth. Overall, this study confirms the effectiveness of rectangular roughness tooth in enhancing shear behaviour.

5.2 Recommendations

Although the current study has successfully investigated the effect of tooth thickness on shear behaviour through a numerical model, further research is recommended to applicability of the findings in real-world scenarios. Firstly, it is recommended to conduct a physical experiment to validate the numerical results. This physical experiment is required as the uncertainty surrounding the suitability of the modelling approach, which utilises a different roughness tooth

shape to calibrate the interface parameter. Thus, a physical experiment is required.

Besides that, future research can also focus on investigating the impact of different tooth shapes, such as trapezoidal, in order to identify the most effective design for maximising shear strength and feasibility. As the rectangular roughness tooth still encounters certain feasibility issues, such as the difficulties during the casting of concrete. The casting of rectangular roughness tooth can be extremely difficult, especially for the top surface, and can easily result in hollowness and seriously affect the overall structural integrity. Therefore, investigating the modified shape of the roughness tooth can offer a better solution and determine whether the trapezoidal roughness tooth can provide improved feasibility compared to the rectangular roughness tooth.

In addition, in order to improve the practicality of the research, future research should focus on integrating reinforcement into concrete specimens. Real-world constructions typically heavily rely on reinforcing elements such as rebar or wire mesh. Including reinforcement as one of the constraints would provide more valuable insight the synergistic effect between roughness tooth and reinforcement in resisting shear forces at the interface. In short, the inclusion of reinforcement marks a significant advancement towards the practical implementation of these findings within the construction industry.

REFERENCES

Ahmed, G.H. and Aziz, O.Q., 2019. Shear behavior of dry and epoxied joints in precast concrete segmental box girder bridges under direct shear loading. *Engineering Structures*, [e-journal] 182, pp.89-100. https://doi.org/10.1016/j.engstruct.2018.12.070.

Al-Fasih, M.Y., Mohamad, M.E., Ibrahim, I.S., Ahmad, Y., Ariffin, M.A.M., Sarbini, N.N., Mohamed, R.N. and Kueh, A.B.H., 2021. Experimental and numerical evaluations of composite concrete-to-concrete interfacial shear strength under horizontal and normal stresses. *PLOS ONE*, [e-journal] 16(5), p.e0252050. https://doi.org/10.1371/journal.pone.0252050.

Ayinde, O.O., Wu, E. and Zhou, G., 2022. Bond behaviour at concrete-concrete interface with quantitative roughness tooth. *Advances in concrete construction*, [e-journal] 13(3), pp.265-279. https://doi.org/10.12989/acc.2022.13.3.265.

Ayinde, O.O., Wu, E., Zhou, G. and Malidadi, T., 2022. Influence of interface roughness geometrical parameters on the shear behaviour of old and new concrete interface. *Asian Journal of Civil Engineering*, [e-journal] 23(2), pp.229-247. https://doi.org/10.1007/s42107-022-00420-4.

Bartels, S., 2016. Finite Element Method. In: *Numerical Approximation of Partial Differential Equations*. [e-journal] Cham: Springer International Publishing. pp.99-152. https://doi.org/10.1007/9783319323541_3.

Dassault Systemes, 2019. *Abaqus 6.11 Documentation*. [online] Abaqus 6.11. Available at: <http://130.149.89.49:2080/v6.11/index.html> [Accessed 9 September 2023].

Demir, A., Ozturk, H., Edip, K., Stojmanovska, M. and Bogdanovic, A., 2018. EFFECT OF VISCOSITY PARAMETER ON THE NUMERICAL SIMULATION OF REINFORCED CONCRETE DEEP BEAM BEHAVIOR. *The Online Journal of Science and Technology*, [e-journal] 8(3), pp.50-56. Available at: <https://www.tojsat.net/journals/tojsat/articles/v08i03/v08i03-09.pdf> [Accessed 16 February 2024].

Dorf, R.C. ed., 2018. *The Engineering Handbook*. 2nd ed. Boca Raton: CRC Press. https://doi.org/10.1201/9781315220338.

Fakeh, M., Jawdhari, A. and Fam, A., 2023. Calibration of ABAQUS Concrete Damage Plasticity (CDP) Model for UHPC Material. [e-journal] https://doi.org/10.21838/uhpc.16675.

Feng, S., Xiao, H., Ma, M. and Zhang, S., 2021. Experimental study on bonding behaviour of interface between UHPC and concrete substrate. *Construction and Building Materials*, [e-journal] 311, p.125360. https://doi.org/10.1016/j.conbuildmat.2021.125360.

Furlong, R., n.d. *Chapter 2 Design for Shear*. [online] Available at: <https://by.genie.uottawa.ca/~murat/Chapter%202%20-%20SHEAR%20DESIGN%20SP%2017%20-%2009-07.pdf> [Accessed 16 July 2023].

Ge, S. and Sinha, S., 2015. Effect of Various Bedding Conditions on Structural Integrity of Prestressed Concrete Cylinder Pipe. *Journal of Materials Science Research*, [e-journal] 4(2). https://doi.org/10.5539/jmsr.v4n2p34.

He, Y., Zhang, X., Hooton, R.D. and Zhang, X., 2017. Effects of interface roughness and interface adhesion on new-to-old concrete bonding. *Construction and Building Materials*, [e-journal] 151, pp.582-590. https://doi.org/10.1016/j.conbuildmat.2017.05.049.

Kuna, M., 2013. Finite Element Method. In: *Finite Elements in Fracture Mechanics: TheoryNumericsApplications*. [e-journal] Dordrecht: Springer Netherlands. pp.153-192. https://doi.org/10.1007/9789400766808_4.

Niwa, J., Fakhruddin, Matsumoto, K., Sato, Y., Yamada, M. and Yamauchi, T., 2016. Experimental study on shear behavior of the interface between old and new deck slabs. *Engineering Structures*, [e-journal] 126, pp.278-291. https://doi.org/10.1016/j.engstruct.2016.07.063.

Parasher, A., 2022. *Shear Force: Definition, Effect, Examples [GATE Notes]*. [electronic print] *byjusexamprep.com*. Available at: <https://byjusexamprep.com/shear-force-i> [Accessed 16 July 2023].

Shamass, R., Zhou, X. and Alfano, G., 2015. Finite-Element Analysis of Shear-Off Failure of Keyed Dry Joints in Precast Concrete Segmental Bridges. *Journal of Bridge Engineering*, [e-journal] 20(6), p.04014084. https://doi.org/10.1061/(asce)be.1943-5592.0000669.

Standard, B., 2004. Eurocode 2: Design of concrete structures. *Part*, *1*(1), p.230.

Wu, E., Ayinde, O.O. and Zhou, G., 2022. Interface Shear Behaviour between Precast and New Concrete in Composite Concrete Members: Effect of Grooved Surface Roughness. *KSCE Journal of Civil Engineering*, [e-journal] 26(6), pp.2799-2812. https://doi.org/10.1007/s12205-022-1173-3.

Wu, E., Ayinde, O.O. and Zhou, G., 2023. Shear behaviour and constitutive model of old-to-new concrete interface with single roughness tooth: Experimental and numerical investigation. *Structures*, [e-journal] 53, pp.1196-1214. https://doi.org/10.1016/j.istruc.2023.05.008.

Xia, J., Shan, K., Wu, X., Gan, R. and Jin, W., 2021. Shear-friction behavior of concrete-to-concrete interface under direct shear load. *Engineering Structures*, [e-journal] 238, p.112211. https://doi.org/10.1016/j.engstruct.2021.112211.

Yuan, Y., Li, M., Alquraishi, A.S.S. and Sun, H., 2021. Experimental Study on the Novel Interface Bond Behavior between Fiber-Reinforced Concrete and

Common Concrete through 3D-DIC. *Advances in Materials Science and Engineering*, [e-journal] 2021. https://doi.org/10.1155/2021/9090348.

Zhao, K., Hu, Z., Wang, B., Li, Q. and Xu, Y., 2023. Effect of roughness and adhesive on the strength of concrete-to-concrete interfaces cast from 3D-printed prefabricated plastic formworks. *Construction and Building Materials*, [e-journal] 368, p.130423. https://doi.org/10.1016/j.conbuildmat.2023.130423.

Zhou, X., Micklebrough, N. and Li, Z., 2005. Shear Strength of Joints in Precast Concrete Segmental Bridges. *ACI Structural journal*, [e-journal] 102(1). https://doi.org/10.14359/13525.

Zhu, Y., Zhang, Y., Hussein, H.H. and Chen, G., 2020. Numerical modeling for damaged reinforced concrete slab strengthened by ultra-high performance concrete (UHPC) layer. *Engineering Structures*, [e-journal] 209, p.110031. https://doi.org/10.1016/j.engstruct.2019.110031.

Zou, Z. and Hameed, M., 2018. Combining interface damage and friction in cohesive interface models using an energy based approach. *Composites Part A: Applied Science and Manufacturing*, [e-journal] 112, pp.290-298. https://doi.org/10.1016/j.compositesa.2018.06.017.

APPENDICES

Appendix A: Compressive and Tensile Behaviour of CDP model

Table A-1: Properties of Old Concrete.

Compressive Behaviour			**Tensile Behaviour**		
Compressive Stress (MPa)	**Inelastic Strain**	**Damage Parameter**	**Tensile stress (MPa)**	**Displacement**	**Damage Parameter**
10.31	0.000000	0.0000	2.77	0.00000	0.0000
11.61	0.000009	0.0000	2.75	0.00017	0.0045
13.51	0.000026	0.0000	2.73	0.00062	0.0119
15.60	0.000053	0.0000	2.68	0.00181	0.0318
17.87	0.000095	0.0000	2.53	0.00501	0.0849
20.25	0.000157	0.0000	2.14	0.01354	0.2266
22.65	0.000248	0.0000	0.55	0.04805	0.8000
24.90	0.000380	0.0000	0.51	0.06296	0.8155
26.76	0.000570	0.0000	0.45	0.08248	0.8358
27.87	0.000838	0.0000	0.38	0.10806	0.8624
27.74	0.001212	0.0047	0.28	0.14157	0.8972
25.69	0.001730	0.0781	0.16	0.18546	0.9429
20.84	0.002438	0.2521			
17.01	0.002883	0.3898			

Table A-2: Properties of New Concrete.

Compressive Behaviour			**Tensile Behaviour**		
Compressive Stress (MPa)	**Inelastic Strain**	**Damage Parameter**	**Tensile stress (MPa)**	**Displacement**	**Damage Parameter**
16.37	0.000000	0.0000	3.68	0.00000	0.0000
18.80	0.000011	0.0000	3.66	0.00019	0.0062
21.51	0.000027	0.0000	3.62	0.00070	0.0166
24.50	0.000053	0.0000	3.52	0.00205	0.0443
27.73	0.000090	0.0000	3.25	0.00567	0.1183
31.15	0.000146	0.0000	2.52	0.01533	0.3160
34.63	0.000227	0.0000	0.74	0.03899	0.8000
37.98	0.000344	0.0000	0.68	0.05109	0.8155
40.85	0.000513	0.0000	0.60	0.06694	0.8358
42.70	0.000757	0.0000	0.51	0.08770	0.8624
42.69	0.001109	0.0002	0.38	0.11489	0.8972
39.49	0.001621	0.0752	0.21	0.15052	0.9429
30.99	0.002365	0.2743			
26.44	0.002685	0.3809			